AD-A108 764 HUGHES RESEARCH LABS MALIBU CA F/G 20/6
POLARIZATION-INDEPENDENT OPTICAL WAVEGUIDE SWITCH.(U)
OCT 81 O G RAMER N00173-80-C-0439
UNCLASSIFIED NL

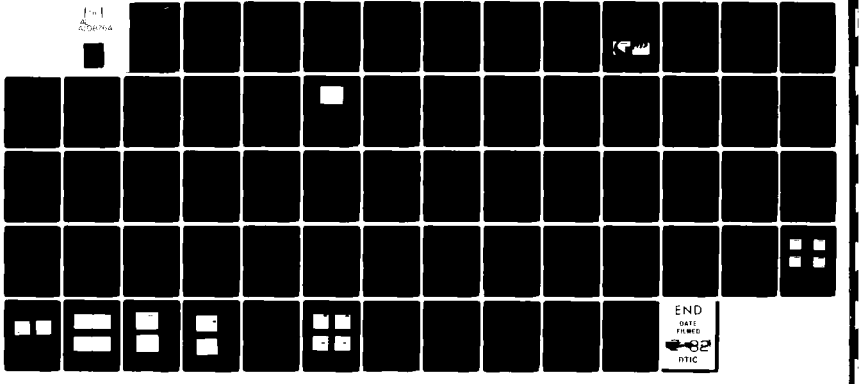

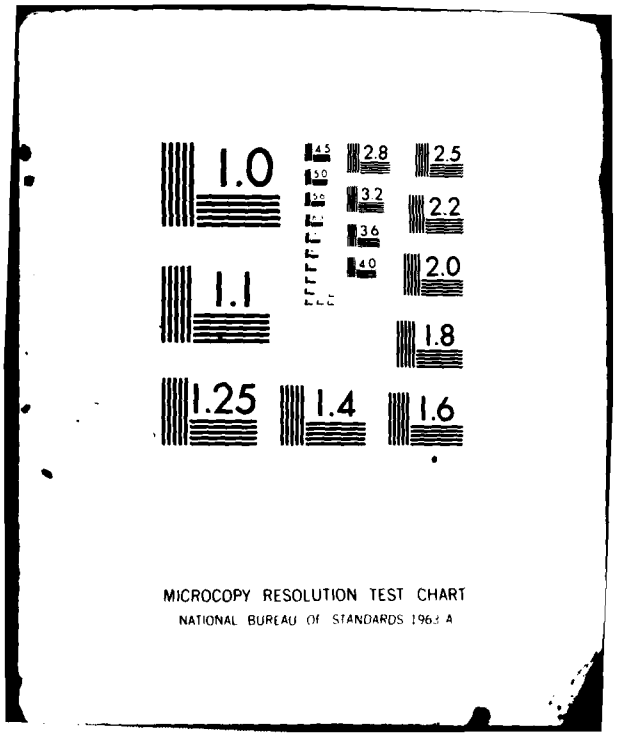
1.0
1.1
1.25
1.4
1.6
1.8
2.0
2.2
2.5
2.8
3.2
3.6
4.0
4.5
5.0
5.6
MICROCOPY RESOLUTION TEST CHART
NATIONAL BUREAU OF STANDARDS 1963 A

POLARIZATION–INDEPENDENT OPTICAL WAVEGUIDE SWITCH

O. G. Ramer

Hughes Research Laboratories
3011 Malibu Canyon Road
Malibu, CA 90265

October 1981

N00173–80–C–0439
Final Report
12 September 1980 – 12 September 1981

Prepared for
NAVAL RESEARCH LABORATORY
Washington, DC 20375

UNCLASSIFIED

SECURITY CLASSIFICATION OF THIS PAGE (When Data Entered)

REPORT DOCUMENTATION PAGE	READ INSTRUCTIONS BEFORE COMPLETING FORM
1. REPORT NUMBER	2. GOVT ACCESSION NO. AD-A108 164
	3. RECIPIENT'S CATALOG NUMBER
4. TITLE (and Subtitle) POLARIZATION-INDEPENDENT OPTICAL WAVEGUIDE SWITCH	5. TYPE OF REPORT & PERIOD COVERED Final Report 13 Sep 1980-13 Sep 1981
	6. PERFORMING ORG. REPORT NUMBER
7. AUTHOR(s) O.G. Ramer	8. CONTRACT OR GRANT NUMBER(s) N00173-80-C-0439
9. PERFORMING ORGANIZATION NAME AND ADDRESS Hughes Research Laboratories 3011 Malibu Canyon Road Malibuk CA 90265	10. PROGRAM ELEMENT, PROJECT, TASK AREA & WORK UNIT NUMBERS
11. CONTROLLING OFFICE NAME AND ADDRESS Naval Research Laboratory Washington, DC	12. REPORT DATE Oct 1981
	13. NUMBER OF PAGES 69
14. MONITORING AGENCY NAME & ADDRESS(if different from Controlling Office)	15. SECURITY CLASS. (of this report) UNCLASSIFIED
	15a. DECLASSIFICATION DOWNGRADING SCHEDULE

16. DISTRIBUTION STATEMENT (of this Report)

This document has been approved for public release and sale; its distribution is unlimited

17. DISTRIBUTION STATEMENT (of the abstract entered in Block 20, if different from Report)

18. SUPPLEMENTARY NOTES

19. KEY WORDS (Continue on reverse side if necessary and identify by block number)

Fiber optics, Integrated optics, Optical processors, Switches

20. ABSTRACT (Continue on reverse side if necessary and identify by block number)

This highly successful program has resulted in the demonstration of an electrically activated planar waveguide polarization independent switch, one of the key components required to implement signal processing components. These switches operate at a wavelength of 0.83 μm and have optical crosstalk values of less than 20 dB. The switch is based on the (Δβ)-reversal directional coupler switch. The polarization independence is incorporated in the (Δβ) reversal switch by tapering the coupling

DD FORM 1 JAN 73 1473 EDITION OF 1 NOV 65 IS OBSOLETE

UNCLASSIFIED

SECURITY CLASSIFICATION OF THIS PAGE (When Data Entered)

delta beta

strength of the directional coupler, and by fabricating the waveguides so that the integrated coupling coefficients for TE and TM modes are nearly identical.

TABLE OF CONTENTS

LIST OF ILLUSTRATIONS

SECTION 1

INTRODUCTION AND SUMMARY

The development of fiber-optic communications as the replacement for coaxial and metal waveguide communication links has demonstrated that high-data-rate capabilties and low-loss propagation of optical signals are feasible. Although most presently envisaged telecommunications systems can be serviced with multi-mode fiber-optic waveguides, specialized high-performance military applications will require single-mode fibers because they offer superior bandwidth and mode control. In addition, single-mode fibers are compatible with single-mode integrated-optics (IO) devices, such as switches. IO switches have been demonstrated with nanosecond speed, drive voltages compatible with semiconductor electronics, and greater than 20 dB isolation. The combination of single-mode fibers and IO switches opens up the opportunity for fiber systems capable of sophisticated optical signal processing. Examples may readily be found in the areas of fiber communications, gyros, and interferometric sensors.

Single-mode fibers actually support two orthogonal modes of polarization. Except for specialized research fibers, these modes are coupled together by small fiber defects, microbends, and environmental perturbations. This mode coupling necessitates that IO switches must switch both polarizations simultaneously if they are to be used with conventional single-mode fibers. In this program, we have designed, fabricated, tested, and delivered to the Navy three electrically activated planar waveguide polarization independent switches. These switches operate at a wavelength of 0.83 μm and have optical crosstalk values of less than 20 dB. One of these four port planar devices is shown in Figure 1. These switches are based on the $\Delta\beta$-reversal directional coupler switch.[1,2] The polarization independence is incorporated in the $\Delta\beta$-reversal switch by tapering the coupling strength of the directional coupler, and by fabricating the waveguides so that the integrated coupling coefficients for TE and TM modes are nearly identical.

The switch development was divided into five phases: coupler characterization (to determine the experimental variation of the coupling constant with guide separation), taper theory studies, switch design, fabrication, and test.

Specific accomplishments made during this program include:

- The design, fabrication, and demonstration of a four-section $\Delta\beta$ reversal polarization independent switch at 0.83 μm wavelength, using a Gaussian taper function.
- An investigation of the filter characteristics of a Gaussian taper function, both theoretically and experimentally.
- The experimental demonstration of Li_2O out-diffused mode elimination, using an H_2O bubbler during Ti in-diffusion process. The devices fabricated for this program have no out-diffused guide.

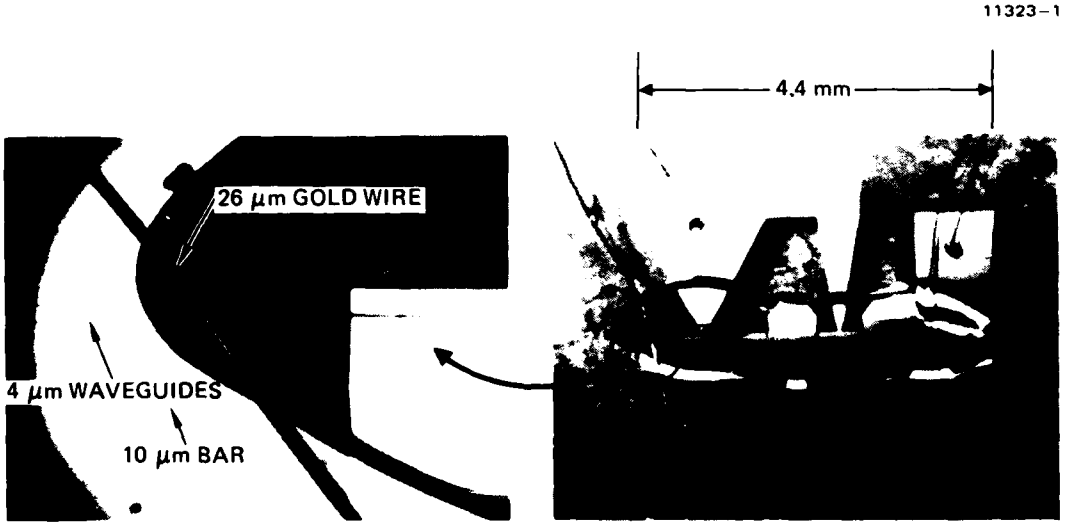

Figure 1. Photograph of polarization independent switch.

Section 2 presents the component design and operation principles for the polarization independent switch. This includes all preliminary coupler characterization data, data associated with out-diffused mode elimination, and theoretical taper studies. Section 3 explains in detail the experimental evaluation performed and the associated test results obtained on each of the three delivered items. In summary, the devices had the following characteristics:

- Cross-state operation with less than 20 V operation and better than 10 dB isolation with no applied voltage.
- Parallel state operation with approximately 100 V applied; voltages larger than 100 V have not been applied due to the possibility of electrode breakdown.

Section 4 outlines the technology development required for significant improvement of the IO chip. The areas where additional research are recommended are:

- Techniques of increasing device length to reduce the switch voltage.
- Development of buffer layers that will allow switch operation at dc.
- Optimization of devices for coupling to optical fibers.
- Deposition of AR coatings on chip edges to eliminate reflections when coupled to fibers.
- Development of methods to measure the differential attenuation associated with the two polarizations (a new noise source to IO circuits).

SECTION 2

COMPONENT DESIGN AND OPERATION PRINCIPLES

A. INTRODUCTION

This section discusses the principles of operation of the $\Delta\beta$-reversal polarization-independent switch. The major difficulty in achieving a polarization-independent directional coupler switch is that the directional coupler's coupling coefficient, κ, and its effective electro-optic coefficients are not identical for both polarizations. As a result, for the same voltage applied to the control electrodes, the induced phase mismatch, $\Delta\beta$, is different for the two polarizations. The values of κ, $\Delta\beta$, and of the coupler interaction length, L, characterize the switch's performance, and therefore its polarization dependence.

The polarization-independent switch fabricated during this program with Ti-diffused $LiNbO_3$ waveguides is shown in Figure 1. It consists of a directional coupler with the coupling coefficient carefully weighted along the length by varying the interguide separation, d. Split electrodes are used to allow application of either the reversed $\Delta\beta$ or the uniform $\Delta\beta$ field configuration.

As in a single polarization switch,[5] the cross-over state, where light incident in one guide emerges in the other guide, is obtained by imposing field polarity changes on the guides, producing the well known $\Delta\beta$-reversal switch. As shown in Figure 2, this is obtained by placing equal and opposite voltages on adjacent electrodes. The straight-through or parallel state where light emerges in the input guide is obtained by placing equal voltages of the same polarity on all electrodes. To obtain a good cross state, the operational conditions require that for both polarizations the integrated coupling coefficient

$$\int_{-L/2}^{L/2} \kappa dz = s \quad , \tag{1}$$

be approximately $\sigma\pi/2$; σ = 1, 3, 5 etc. This corresponds to a device with 1, 3, 5, etc. complete optical transfers between the waveguides, (i.e., an approximate cross-state). This constraint is primarily associated with the effect of the applied electric field on the two polarizations. For a Z-cut crystal orientation and the electrode placement illustrated in Figure 2, we can write

$$\Delta\beta_{TE} \propto n_o^3 r_{13} V \quad , \tag{2}$$

and

$$\Delta\beta_{TM} \propto n_e^3 r_{33} V \quad , \tag{3}$$

where V is the applied voltage, n_e and n_o are the ordinary and extraordinary refractive indices, and the electro-optic coefficients have the ratio, $r_{33}/r_{31} \approx 3$ (Ref. 3). For single-mode waveguides, this implies $\Delta\beta_{TM}/\Delta\beta_{TE} \approx 2.67$, when crystal birefringence is taken into account.

The integrated coupling strengths for the TE and TM modes can be made equal for Z-cut $LiNbO_3$ by an appropriate choice of waveguide and coupler parameters.[4] Briefly, we find experimentally that the coupling strength for either polarization can be written approximately as

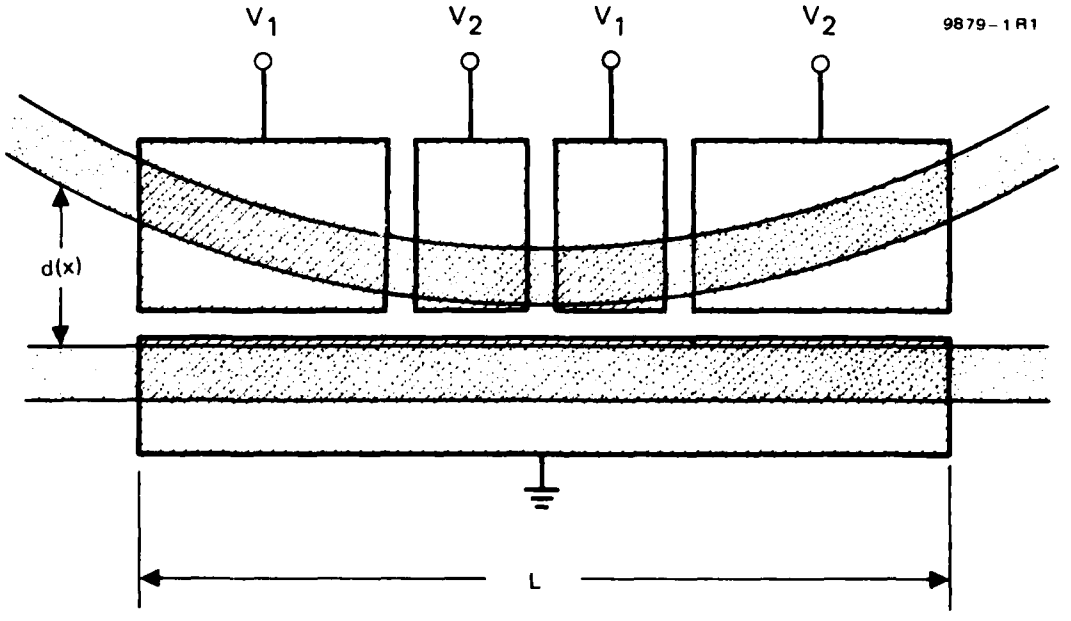

Figure 2. Diagram of Δβ-reversal polarization-independent switch.

$$\kappa = \kappa_o \exp \frac{-d}{\gamma} \quad , \tag{4}$$

where d is the interguide separation, and γ is the waveguide mode lateral evanescent penetration depth. The parameters κ and γ are, in general, unequal for the two modes, resulting in an intersection of $\kappa_{TE}(d)$ and $\kappa_{TM}(d)$. Due to this intersection, the integrated coupling strength for the tapered directional coupler, s_{TE} and s_{TM}, can be approximately equalized for the tapered couplers.

To understand how dual-polarization operation is obtained for the cross-over state, the theoretical cross-state switching curve for a 2 section switch is shown in Figure 3. This curve specifies, for a given s, the required $\pm\Delta\beta L$ over the two sections to achieve a perfect cross-over state. The results were calculated by Alferness[1] using a Hamming weighting for the tapered coupler. The dashed curves in Figure 3 indicate the -20 dB crosstalk limits. The switch is designed with $s_{TM} \simeq s_{TE} \simeq \pi/2$, as shown in Figure 3. For these values of s, the required $\Delta\beta_{TM}L$ to switch the cross-over state is 2.7 times the required value of $\Delta\beta_{TE}L$ to switch the same state with better than -20 dB crosstalk. Thus, for the same applied voltage, both modes approximately satisfy the cross-state condition. Precise values of s are not necessary. No more than 20% accuracy is needed, which is within fabrication limits.[1]

The straight-through state is obtained by applying the same voltages to all electrodes, thereby creating a uniform phase mismatch along the tapered coupler. The straight-through state can be obtained even with large differences in electro-optic effect because a tapered directional coupler is used. Figure 4 shows the power in the cross-over guide of a Hamming-tapered coupler as a function of normalized phase mismatch, δL, where $\delta = \Delta\beta/2$. The effect of the taper is to keep the response side lobes down (typically, as much as -25 dB) as the phase mismatch is increased. Thus, to obtain the straight-through state requires increasing the applied voltage until the response is in the low-side-lobe regime for both polarizations.

B. CHANNEL WAVEGUIDE FORMATION IN $LiNbO_3$

Low-loss single-mode optical channel waveguides are fabricated in $LiNbO_3$ substrates by the in-diffusion of titanium metal. The presence of Ti ions increases the polarizability of the medium, thus generating a region of higher index of refraction.

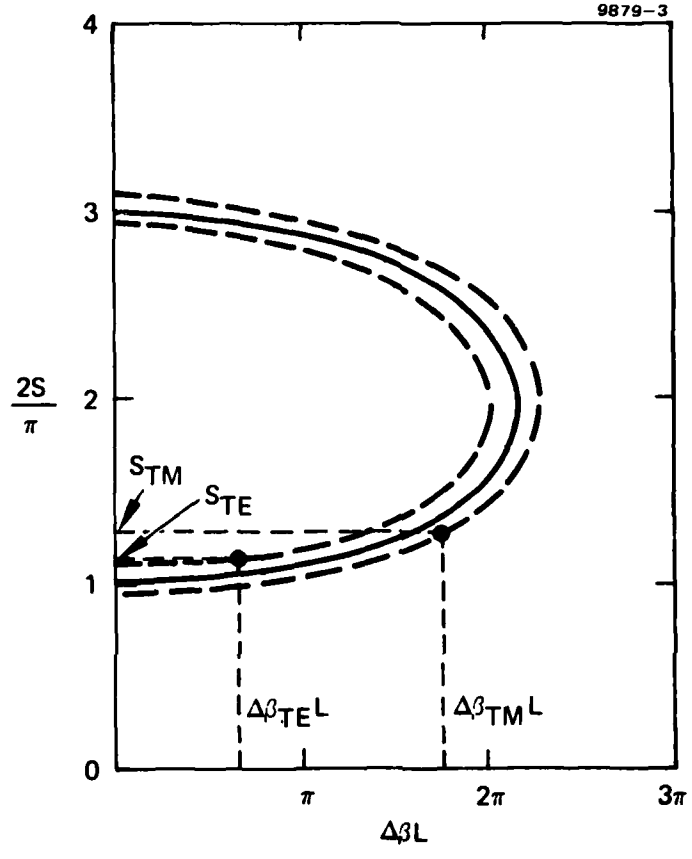

Figure 3. Cross-bar diagram of a Hamming tapered directional coupler switch.

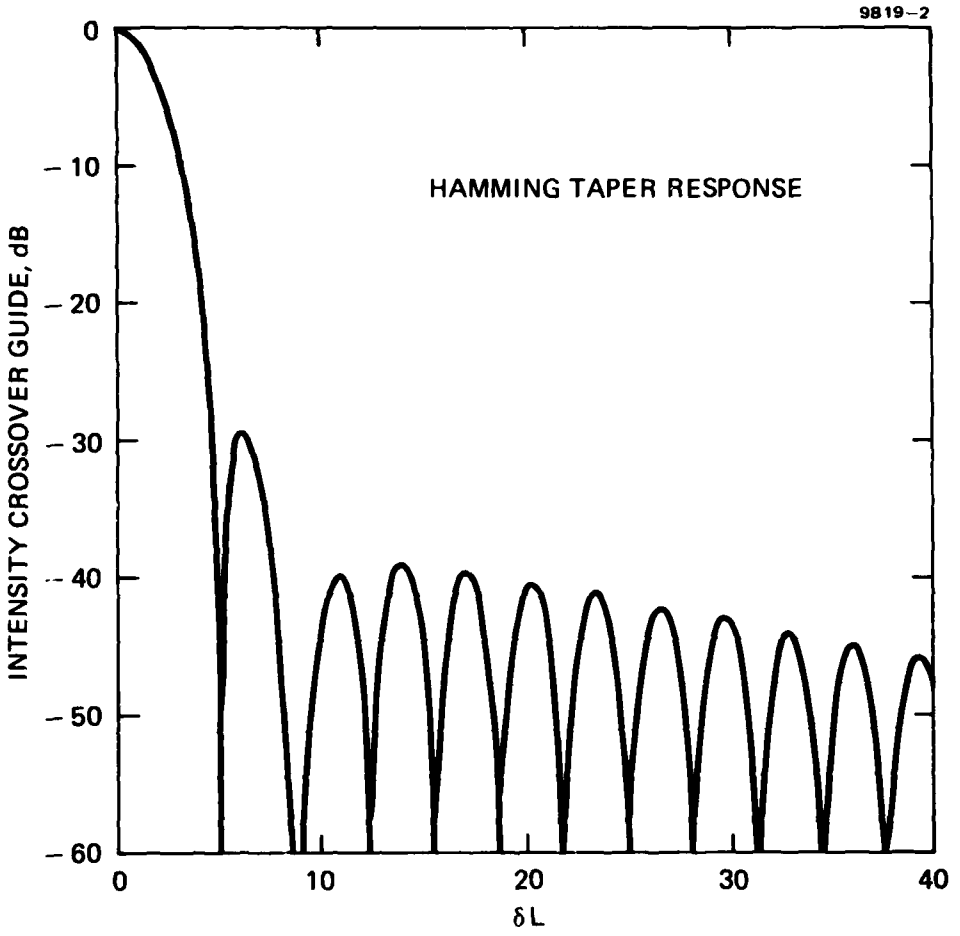

Figure 4. Response of a Hamming tapered directional coupler as a function of normalized phase mismatch, δL.

By adjusting the thickness and the width of the Ti channel, single-mode optical waveguides in both the transverse and depth directions are easily obtained.

Photolithographic techniques are used to define the Ti pattern. These techniques include sputter etching, chemical etching, and photoresist liftoff. At HRL, the photoresist lift-off technique is used to form the desired Ti pattern because it provides a better edge definition of Ti channels. During the fabrication process, the pattern of single-mode channel waveguides are first delineated on the positive Shipley AZ 1305B photoresist. After exposing and developing the photoresist, a 200- to 600-Å-thick Ti film is electron-beam (E-beam) deposited onto the photoresist pattern for guides. The open area is thus filled with Ti metal. The unwanted Ti coating on the photoresist is removed by dissolving the photoresist underneath in acetone. The in-diffusion process is performed in a flowing gas atmosphere at a temperature between 900 and 1000°C. In order to eliminate the Li_2O outdiffused mode, the flowing gases are H_2O-saturated Ar during diffusion, and H_2O-saturated O_2 during cool down. The diffusion time is 6 to 8 hrs. Before diffusion, the Ti metal is oxidized to TiO_2 at 600°C. The addition of the oxidation step before diffusion enhances the surface quality of the sample and the reproducibility of the diffusion process.

During E-beam evaporation, the thickness of the Ti film is monitored by a quartz crystal oscillator. After diffusion, waveguide ridges about 2.5 times as high as the original Ti thickness are present. These ridges are used as registration marks in later photolithographic processing.

C. Li_2O OUT-DIFFUSION MODE ELIMINATION

Since this program involved devices requiring polarization independence, it was felt that the best possible device would be one without an Li_2O out-diffusion planar mode. Alferness[6] and Jackel[7] et. al. reported out-diffusion elimination by adding water vapor to the diffusion gases. We have duplicated these results during this program and in the process discovered some interesting phenomena. Our first experiment was to use only flowing O_2, without using any argon. The result of this first diffusion of four samples with equal Ti depth was surprising; the modal characteristics of the four samples were different (see Table 1). Since these experiments, HRL has successfully eliminated out-diffusion with only $O_2 + H_2O$ under another program. In the second series of experiments, we used the Ar and O_2 combination of gases reported by Alferness.[6] This resulted

in samples with and without out-diffusion, but no significant modal dispersion from sample to sample. The samples with an outdiffusion mode were either from a single sample diffusion, or the first sample along the gas flow direction.

The gas flow rates, H_2O concentration, and the sample position relative to other samples have been identified as important parameters in the out-diffusion process. In our experiments we used the following conditions: (1) a one liter/min flow rate, (2) a 3 in. quartz tube, and (3) the partial pressure of H_2O at room temperature. If devices are to be fabricated at Naval Research Laboratories with the supplied masks, it is recommended that these conditions be matched as closely as possible.

A photograph of the edge of one of the delivered devices under both TE and TM excitation is shown in Figure 5. Note the absence of the out-diffused mode.

Table 1

Mode / Sample	TE	TM
19	mm-sm	mm-sm
20	sm	mm
21	sm	sm
22	co	sm

co = cutoff; mm = multimode; sm = single-mode; mm-sm = some single, some multimode.

11323-16

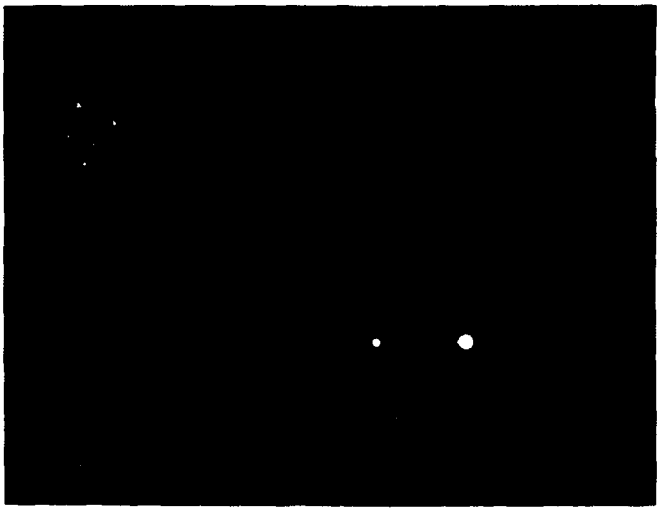

Figure 5. A photograph of the edge of one of the delivered devices under both TE and TM excitation. Note the absence of the out-diffused mode.

D. COUPLER CHARACTERIZATION

Since there is no analytical description for the modal field of a single diffusion channel waveguide, no closed-form expression for the coupling length, ℓ, is available for directional couplers. However, the coupling between two uniform index channel waveguides has been analyzed.[8] In this case,

$$\ell = \ell_0 \exp \frac{d}{\gamma} , \tag{5}$$

where ℓ_0 depends on the waveguide parameter, but is independent of d, the separation between guides. The quantity γ is the evanescent penetration depth. Qualitatively, ℓ_0 depends on the shape of the fields within each guide.

It has been shown during this program that the relationship given by Equation (5) also is obeyed for diffused channel waveguides. The quantities ℓ_0 and γ have to be determined experimentally. A significant portion of the program was dedicated to making these measurements. This is partially due to our experiments on Li_2O out-diffusion elimination.

The method for determining the coupling coefficient, $\kappa = \pi/2\ell$ is illustrated in Figure 6. The output intensity from the two channels, assuming only one has been excited, is proportional to $\sin^2(\kappa L + \phi)$ and $\cos^2(\kappa L + \phi)$, where κ is the coupling coefficient, L is the interaction length, and ϕ is the amount of coupling that has taken place in the transition to and from the interaction region. Thus,

$$\kappa L + \phi = \tan^{-1}(\sqrt{\text{ratio}}) \quad , \tag{6}$$

where ratio = the ratio of the two output intensities. During this program we generated a number of samples for characterization of the transfer length (Figure 7). We covered a large range of Ti concentrations and gas flow conditions. In all cases, the intersection of the TE and TM ℓ vs d curves was not appropriate for the successful fabrication of a $\pi/2$ switch. (The required switch voltage would have been excessive.) The approach taken to reduce the switch voltage is described in the following subsection, as is the taper theory.

E. DESIGN CHARACTERISTICS OF A POLARIZATION INDEPENDENT OPTICAL SWITCH USING A GAUSSIAN TAPER FUNCTION

The filter characteristics of smoothly weighting or tapering the coupling between codirectional interacting waveguides and contradirectional Bragg reflection devices have been studied and reported.[9-14] Filters of both types have promise for use in integrated optical waveguide circuits for light-wave communications. Specific applications that have been identified are wavelength multiplexers or demultiplexers,[14] polarization-independent optical switches or modulators,[1] and Bragg mirrors.[10]

Examples of both the codirectional and contradirectional filters are shown in Figure 8. The interaction between the two modes in either device is described by a nonlinear Ricatli equation.[9,11] In general, the local coupling between the modes is described by a coupling coefficient, $\kappa(z)$. Several functional relations for $\kappa(z)$ have been studied for their filter characteristics. The ones producing the lowest sidelobe levels to date have been a set of "window" functions that have been thoroughly studied for their properties as digital filters.[12] In this report we consider a truncated Gaussian to describe the functional behavior of $\kappa(z)$.

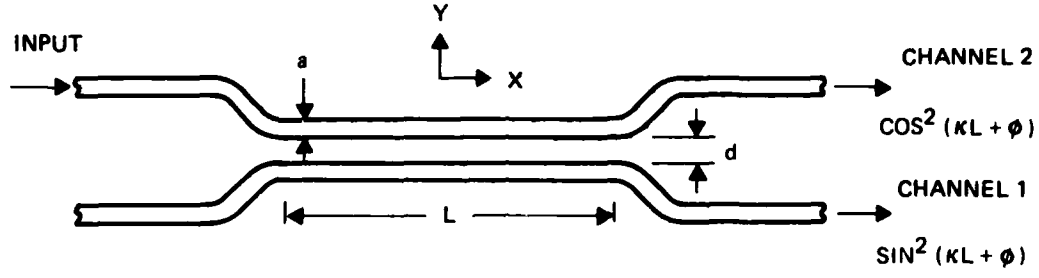

κ = COUPLING COEFFICIENT

L = INTERACTION LENGTH

φ = TOTAL COUPLING IN TRANSITION REGIONS

$$\kappa L + \phi = \tan^{-1}\left(\frac{I_{CHANNEL\ 1}}{I_{CHANNEL\ 2}}\right)^{1/2}$$

ON MASK L = 1, 1.5, 2, 2.5, 3, 3.5, 4, 4.5, 5 AND 7.5 mm
d = 2, 3, 4, 5, 6 μm
a = 4 μm

Figure 6. Method for determining the coupling coefficient, κ.

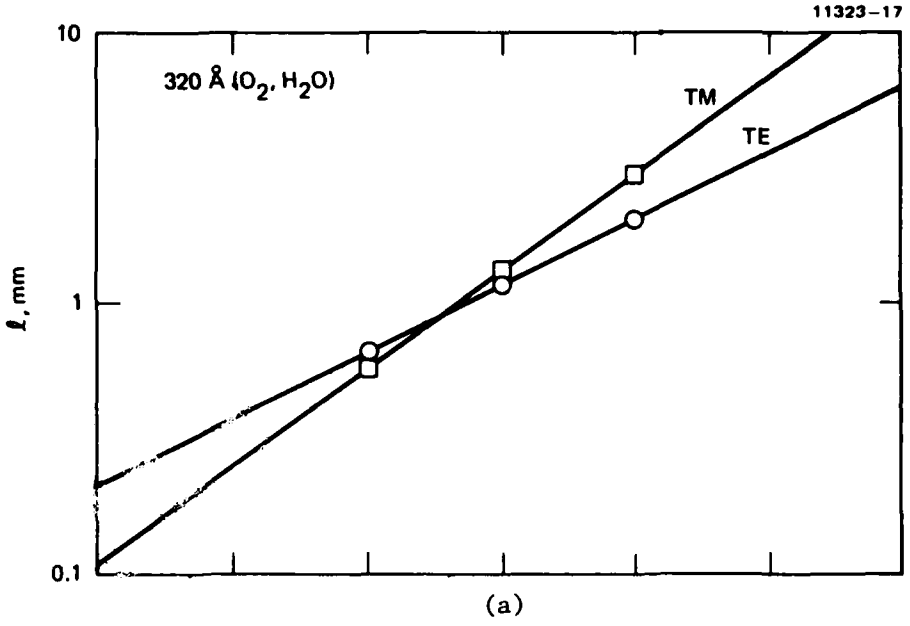

(a)

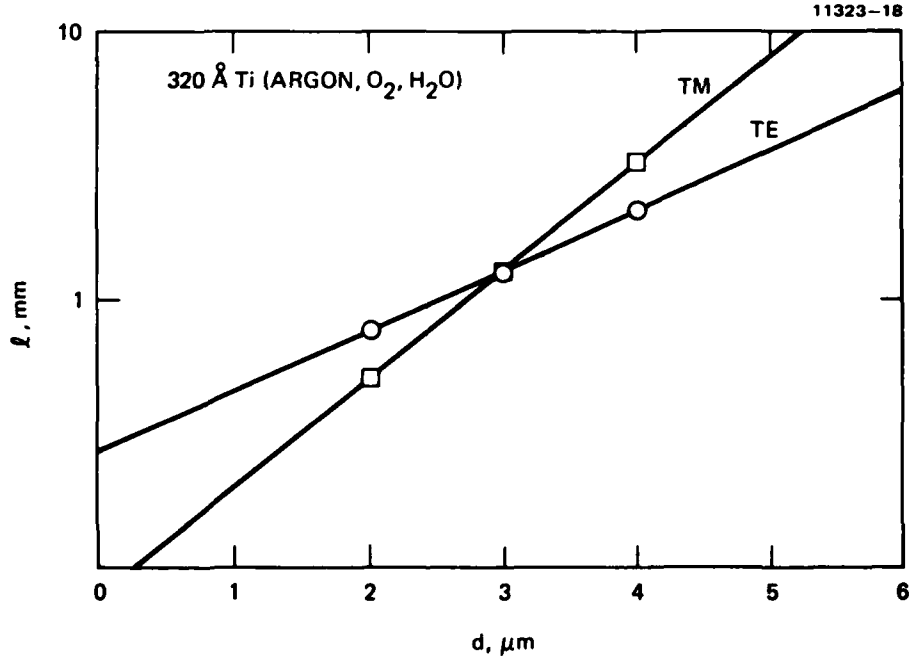

(b)

Figure 7. Example of ℓ vs. d behaviors for several samples.

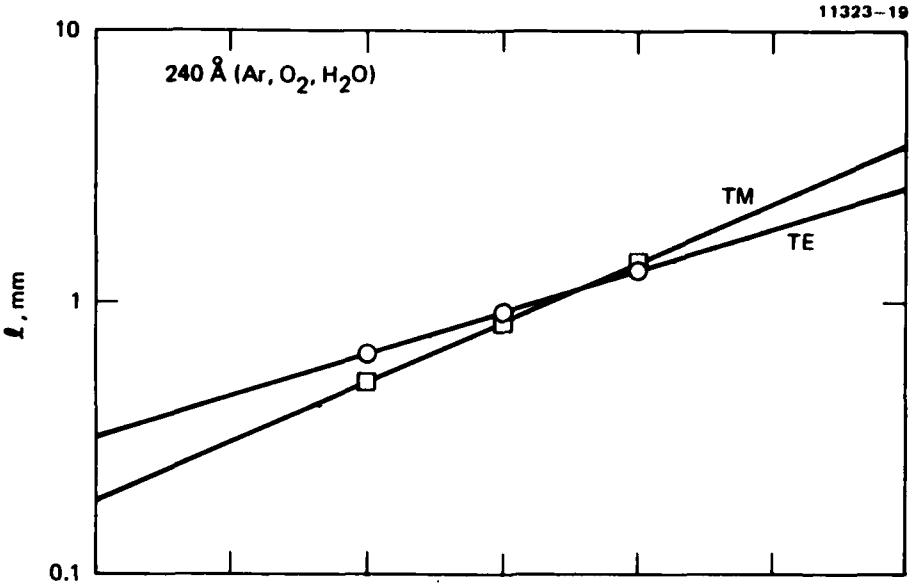

(c)

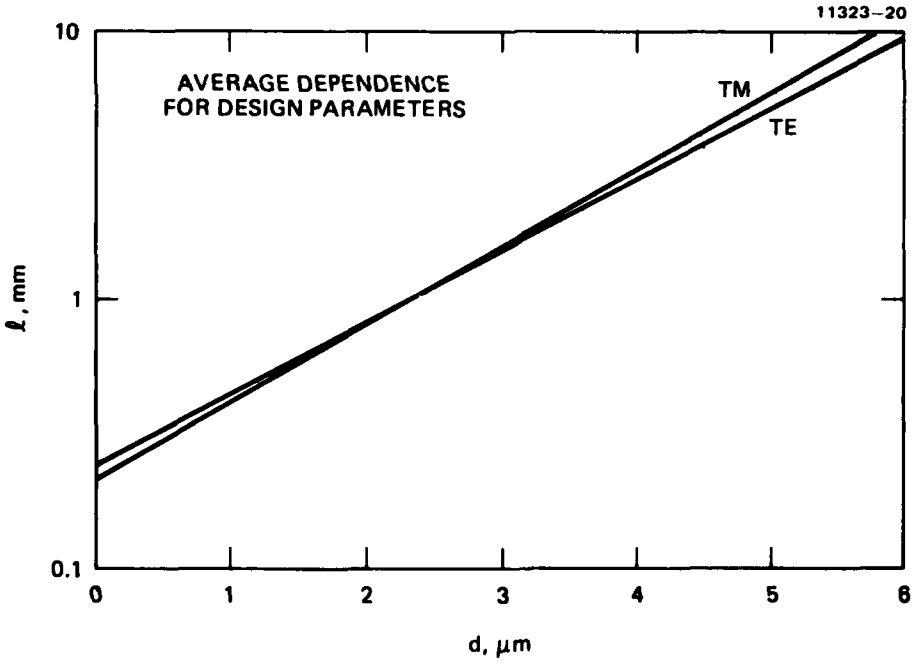

(d)

Figure 7. Continued.

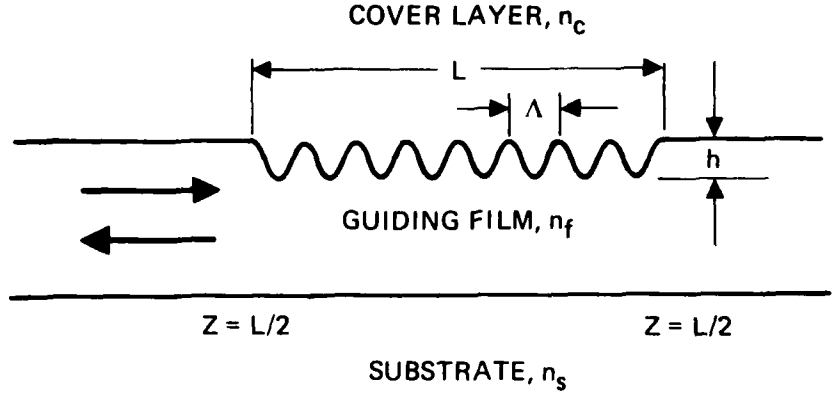

(a) CONTRADIRECTIONAL BRAGG REFLECTOR

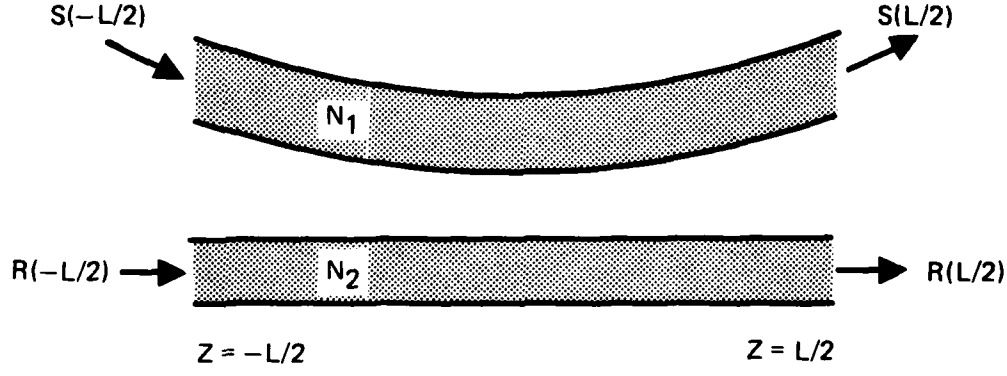

(b) CODIRECTIONAL INTERACTING WAVEGUIDES

Figure 8. Diagram of coupled optical modes.

Of primary consideration in this section is the codirectional case, along with the design of a polarization-independent switch using the Gaussian taper function and multiple sections of $\Delta\beta$ reversal at a wavelength of 0.83 μm. This work follows that of Alferness[1] who worked at a wavelength of 0.63 μm and used a single section $\Delta\beta$ reversal and the Hamming taper function. Fortunately, $LiNbO_3$ does not suffer from the extreme optical damage at $\lambda = 0.83$ μm that exists at $\lambda = 0.63$ μm, which makes the switch designed here potentially useful in optical communication systems.

1. Gaussian Taper Function

The interaction between the two modes in either of the codirectional or contradirectional device is described by a nonlinear Ricaiti equation:[9,11]

$$\rho' = (\pm)j(2\delta(\mp)\phi')\rho + j\kappa((\pm)\ 1 + \rho^2) \tag{7}$$

$$\rho = \frac{S}{R} e^{-j\phi} \quad , \tag{8}$$

where the lower and upper signs correspond to the codirectional and contradirectional devices, respectively; R and S are the slowly varying amplitudes of the incident and cross-over waves; and $\delta = \Delta\beta/2$ (where $\Delta\beta = \beta_2 - \beta_1$ or $\Delta\beta = \beta_2 - \beta_1 - 2\pi/\Omega$ when a periodic modulation of β or κ is used to achieve phase matching). The function, $\phi(z)$, is a measure of the spatial variation in the phase match condition, similar to that in the chirp function in the contradirectional case, or a spatial variation of the effective guide indices in the codirectional case. The boundary condition for this equation is

$$\rho[(\pm)L/2] = 0 \quad , \tag{9}$$

where the lower and upper sign corresponds to the codirectional and contradirectional devices, respectively, and L is the length of the device (see Figure 8). The customary numerically determined value for the codirectional and contradirectional cases are

$$|S|^2 = \frac{\rho^2}{1 + \rho^2} \quad , \tag{10}$$

and the reflectivity, is

$$\left|\frac{R}{S}\right|^2 = \rho\rho^* \quad . \tag{11}$$

Several functional relations have been used for $\kappa(z)$ by previous authors.[9-13] In general,

$$\kappa(z) = sw(z)/L \quad , \tag{12}$$

where the taper function, $w(z)$, is normalized so that

$$\int_{-L/2}^{L/2} w(z)dz = L \quad , \tag{13}$$

and the integrated coupling length is s. The functions producing the lowest sidelobe levels to date have been a set of "window" functions that have been studied for their properties as digital filters, with finite impulse response and minimal Fourier transform sidelobes.

The function investigated in this study has been a truncated Gaussian function,

$$w(z) = \frac{2\alpha}{\sqrt{\pi}} e^{-(2\alpha z/L)^2} \Big/ \operatorname{erf}(\alpha) \quad . \tag{14}$$

This function has also been normalized in correspondence to Equation (13).

The truncated Gaussian has been utilized because of the very low Fourier transform sidelobe that can be achieved. For the non-truncated Gaussian ($\alpha = \infty$) the Fourier transform is another Gaussian which does not contain sidelobes. For the truncated Gaussian, the value of α can be used as a variable in obtaining the desired sidelobe level and in optimizing the filter response. The calculated filter responses for a codirectional coupler with $s = \pi/2$, $3\pi/2$, and $5\pi/2$ are shown in Figure 9. The parameter in each figure is the truncated factor, α. It is clear that a wide range of filter responses can be obtained by varying the truncation parameter, α.

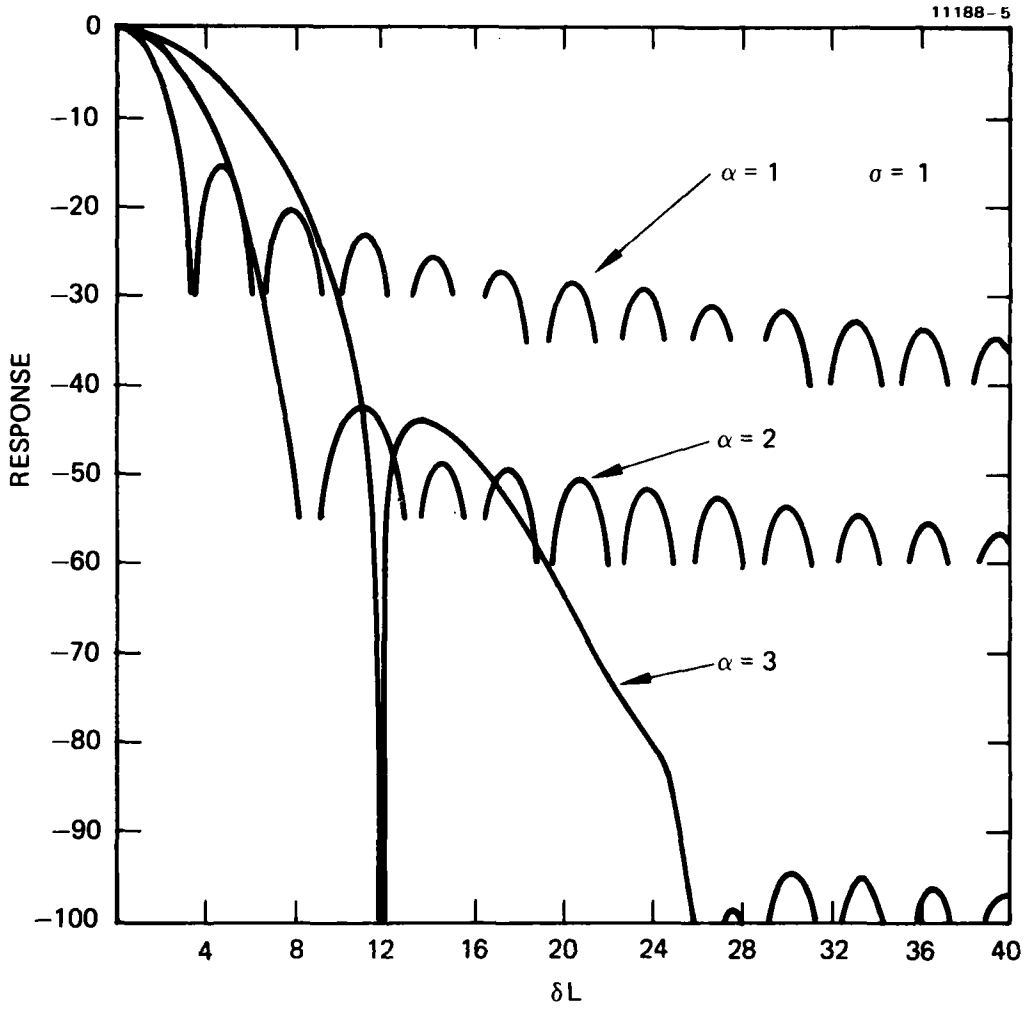

Figure 9(a). Truncated Gaussian taper codirectional filter response with $\alpha = 1, 2, 3$, and $\sigma = 1$.

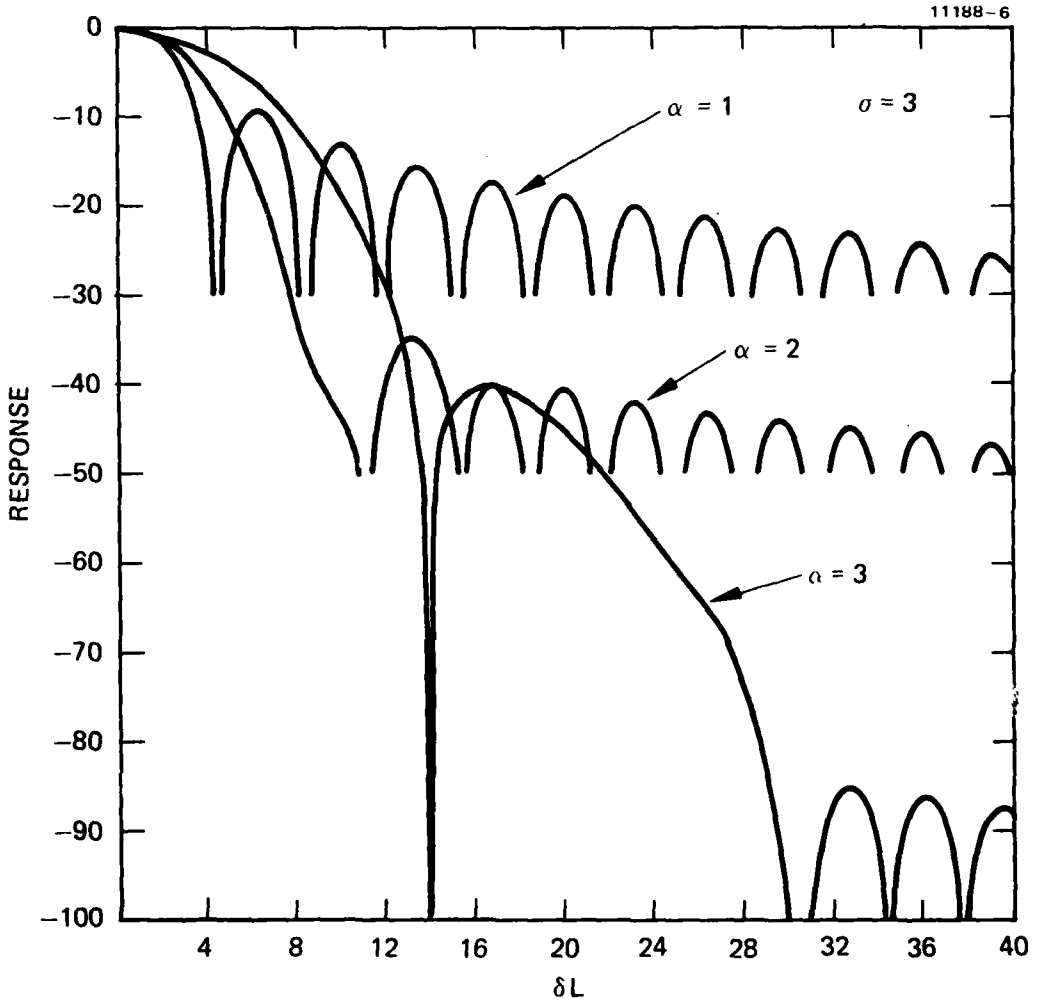

Figure 9(b). Truncated Gaussian taper codirectional filter response with $\alpha = 1$, 2, and 3, and $\sigma = 3$.

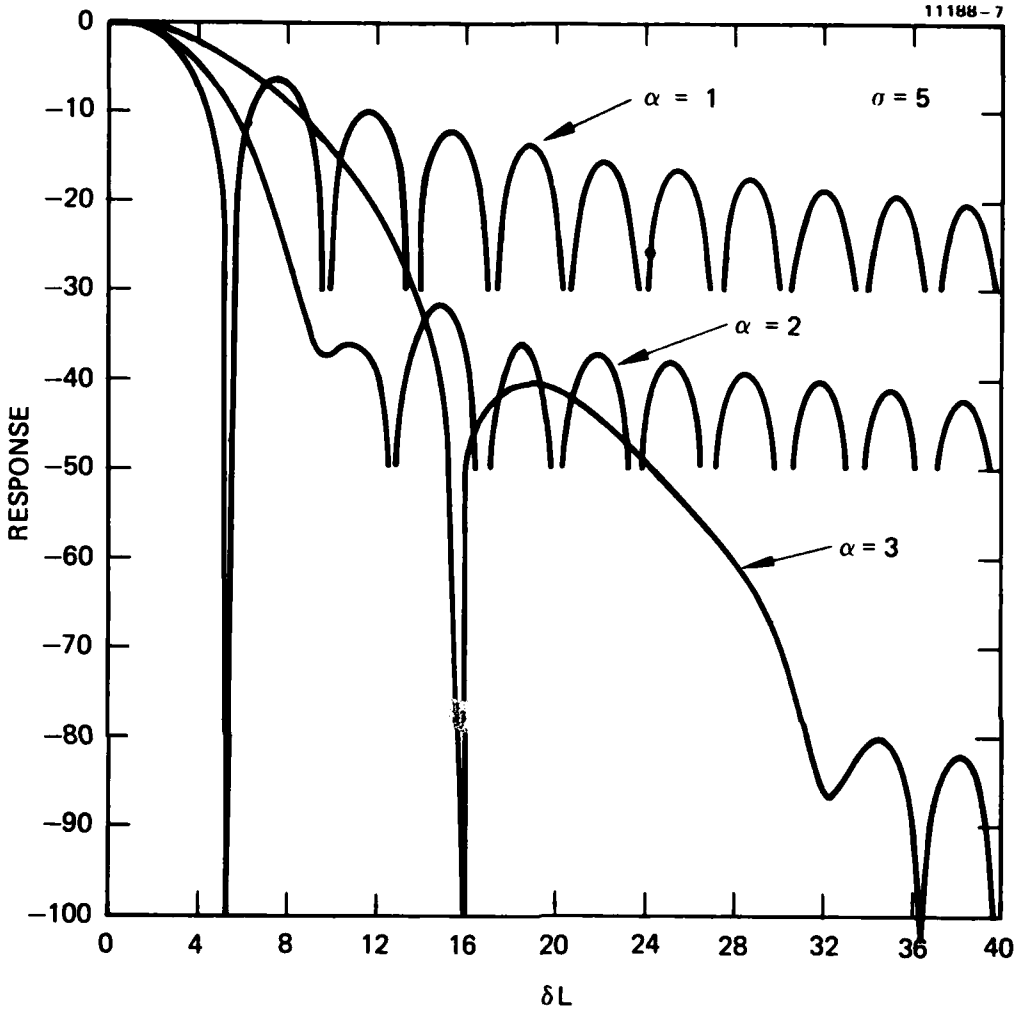

Figure 9(c) Truncated Gaussian taper codirectional filter response with $\alpha = 1$, 2, and 3, and $\sigma = 5$.

In order to fabricate a codirectional filter, it is necessary to design a mask that will result in waveguides having the desired variation of $\kappa(z)$. This design is constrained by the mask or pattern generator and will result in an approximate Gaussian variation of $\kappa(z)$, assuming the exact dependence of κ versus waveguide separation is known. Typically, pattern generators have 0.1° angular resolution and 0.1 to 0.5 μm displacement resolution. With these constraints, two possible "fits" to the Gaussian are tangential segments at 0.1° angular increments, and parallel (0°) segments displaced by an amount equal to the resolution of the pattern generator. The former fit produces the minimum number of discrete discontinuities in the waveguide. Effects on the filter characteristics due to fitting[12] will be shown after the switch design details are discussed below.

Since there is no analytical description for the modal field of a single mode diffused channel waveguide, no closed-form expression for the coupling coefficient, κ, is available for codirectional couplers. However, the coupling between two uniform index channel waveguides has been analyzed.[8] In this case,

$$\kappa = \kappa_o e^{-d/\gamma} \quad , \tag{15}$$

where κ_o depends on waveguide parameters, but is independent of d, the separation between guides. The quantity γ is the evanescent penetration depth. Experiments have shown that an identical relationship exists for Z-cut $LiNbO_3$:Ti-diffused guides.[15] Therefore, given κ_o, γ, α, s, and L, the d(z) can be determined:

$$d(z) = -\gamma \ln(sw(z)/L\kappa_o) \quad . \tag{16}$$

In order to fit the taper with angular incremented segments, the tangential points must be determined. For the Gaussian dependence of $\kappa(z)$, the position where the taper function has a slope

$$m = \frac{dd}{dz} \quad , \tag{17}$$

is

$$z(m) = L^2 m/8\gamma\alpha^2 \ . \tag{18}$$

Finally, in order to fit the curve with incremental steps or parallel segments, the position z(d) where the incremental steps occur must be determined. Therefore, we apply

$$z(d) = \frac{\pm L}{2\alpha} \sqrt{\frac{d}{\gamma} + \ln \left(\frac{2\alpha s}{\pi \mathrm{erf}(\alpha)\ L\ \kappa_o} \right)} \ . \tag{19}$$

2. Polarization Independent Optical Switch (PIOS) Design

In general, the coupling coefficient for the two polarizations of $LiNbO_3$:Ti-diffused waveguides are unequal. At a narrow waveguide separation, the coupling coefficient for the TE polarization is typically larger than that for the TM polarzation. The reverse is typically true for wider waveguide separations. This situation makes it possible to design a tapered waveguide system so that

$$\int_{-L/2}^{L/2} \kappa_{TE} dz = \int_{-L/2}^{L/2} \kappa_{TM} dz = s \tag{20}$$

by digitally determining the appropriate length, L, of the device. This capability is basically the requirement to achieve a cross-state in the polarization-independent optical switch considered in this report. The parallel state is obtained by relying on the filter response of the device.

As pointed out by Alferness,[1] the requirements for the PIOS design include: for the cross-state,

$$s \approx \sigma\pi/2 \qquad \sigma = (1,\ 3,\ 5, \ldots) \ , \tag{21}$$

and for the parallel state,

$$\kappa_{TM} = sw(z)/L \ . \tag{22}$$

The taper function, w(z), is constrained to functions having low Fourier transform sidelobes. In our design the taper function utilized is the truncated Gaussian discussed earlier. The switch demonstrated by Alferness had a $\sigma \approx 1$. The remainder of this section deals with the design characteristics of switches with $\sigma > 1$. Variations from the $\sigma = 1, 3, 5...$condition in the device can be adjusted by the $\Delta\beta$ reversal electrode in a fashion similar to that explained by Alferness.

For a truncated Gaussian function, the value of α can be used as a variable in optimizing the filter response. Some of the factors involved in the selection of α are plotted in Figure 10. This data was generated using experimentally determined values of γ and k (Table 2); the waveguides were fabricated on Z-cut $LiNbO_3$ using 360 Å Ti and a 1000°C, 8 hr diffusion; the experimentally determined values of γ and κ (Table 2); the waveguides were fabricated on Z-cut $LiNbO_3$ using 360 Å Ti and a 1000°C, 8 hr diffusion; the Li_2O out-diffusion mode was eliminated by using a water bubbler and flowing Ar during diffusion, and flowing O_2 during cool down.

The interaction length, L, is plotted in Figure 10(a). More important, however, is the value of δ at -20 dB optical crosstalk (the design goal for the switch), which is proportional to the required switch voltage (Figure 10(b)). The minimum and maximum (Figure 10(c)) guide separation are important dimensions in the PIOS design; the coupling length versus guide separation is plotted in Figure 7. In general, the smaller the α, the lower the switch voltage; however, α must be large enough so that at d_{max} the guides approximate the condition, $\kappa(d_{max}) = 0$.

Table 2. Design Waveguide Parameters

Mode Parameters	k_o μm^{-1}	γ μm^{-1}
TE	6.44	1.64
TM	7.22	1.52

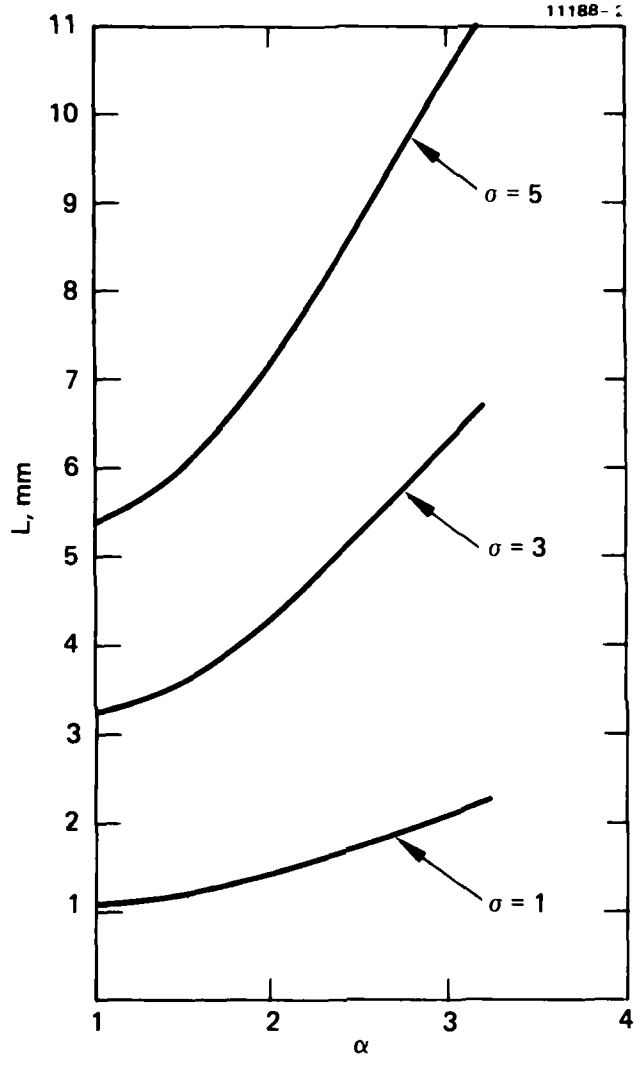

Figure 10(a). Plot of interaction length versus the truncation factor α; the parameter is $2s/\pi = \sigma$.

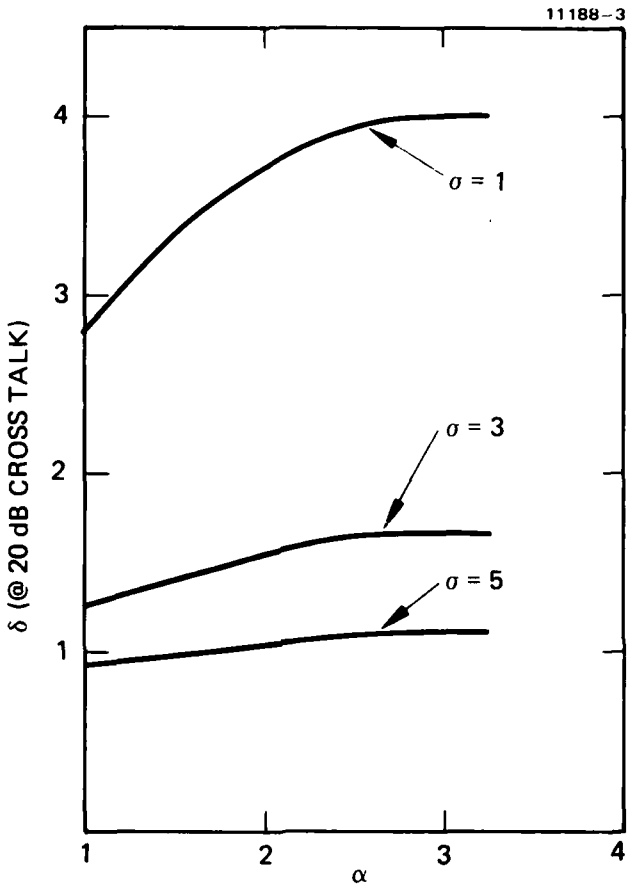

Figure 10(b). The required δ applied to achieve 20 dB optical crosstalk in the parallel state versus the truncation factor, α; the parameter is $2s/\pi = \sigma$

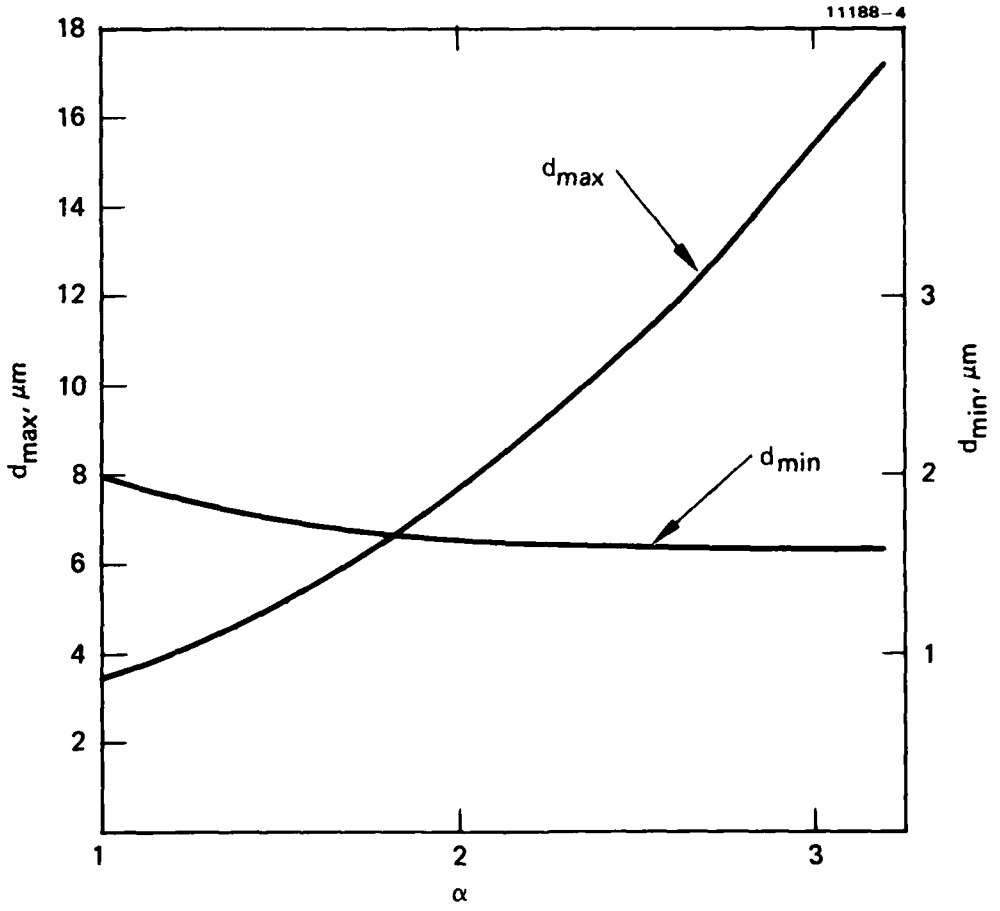

Figure 10(c). The minimum and maximum guide separations versus the truncation function α; these dimensions are independent of $2s/\pi = \sigma$.

The other necessary selection in the design of a PIOS is σ (see Equation (17)). Increasing σ increases the device length; in fact, $L_\sigma = \sigma L_1$. The longer the device, the lower the required switch voltage; but the voltage does not drop as (σ^{-1}). Plotted in Figure 9 is the filter response for $\sigma = 1,3,5$ (in the associated calculations, $L_\sigma = \sigma L_1$). The associated δ's for -20 dB crosstalk for the TE polarization versus the value of α, with σ as a parameter, is plotted in Figure 10(b) ($\Delta\beta_{TM} = 2.67 \times \Delta\beta_{TE}$ for Z-cut $LiNbO_3$ at 0.83 μm wavelength). It is apparent that for higher σ's the switch voltage is reduced; i.e., reduced δ. The final consideration in the selection of σ is the response after fitting the truncated Gaussian to what can be achieved by mask making. Plotted in Figure 11 for $\alpha = 2$ are the filter responses for $\sigma = 1$, 3, and 5 using 0.1° angularity incremented segments to approximate the taper function. The ideal responses are given in Figure 9. The very obvious degradation at $\sigma = 3$ and 5 is associated with the accuracy to which the angular segments can approximate the taper function. As σ increases, the number of segments decrease on the same order as $1/\sigma$, since the length of interaction increases on the same order as $L = \sigma L_1$, but d_{min} and d_{max} remain constant.

If values of $\sigma > 3$ are required (for example, to reduce the switch voltage), one has to consider fabricating the mask using parallel segments displaced by an amount equal to the resolution of the pattern generator. Thus, for 0.1 μm displacements between segments and $\alpha = 2$, the filter response for $\sigma = 5$ is plotted in Figure 12. For this technique, the number of parallel segments remain constant as σ increases; however, the segment length is proportional to σ. The primary disadvantage of this approach is the large number of discrete waveguide discontinuities and mask fabrication complexity.

F. WAVEGUIDE MASK DESIGN

The switch waveguide mask was designed with the mask digitization and fabrication capabilities of Electromask in mind. At the time of the design, the capabilities were 0.5 μm displacement resolution for a device of this length and 1.0° angular resolution. With these constraints, two possible "fits" to the Gaussian were tangential segments at 0.1° angular increments, and parallel (0°) segments displaced by an amount equal to the resolution of the digitization. The

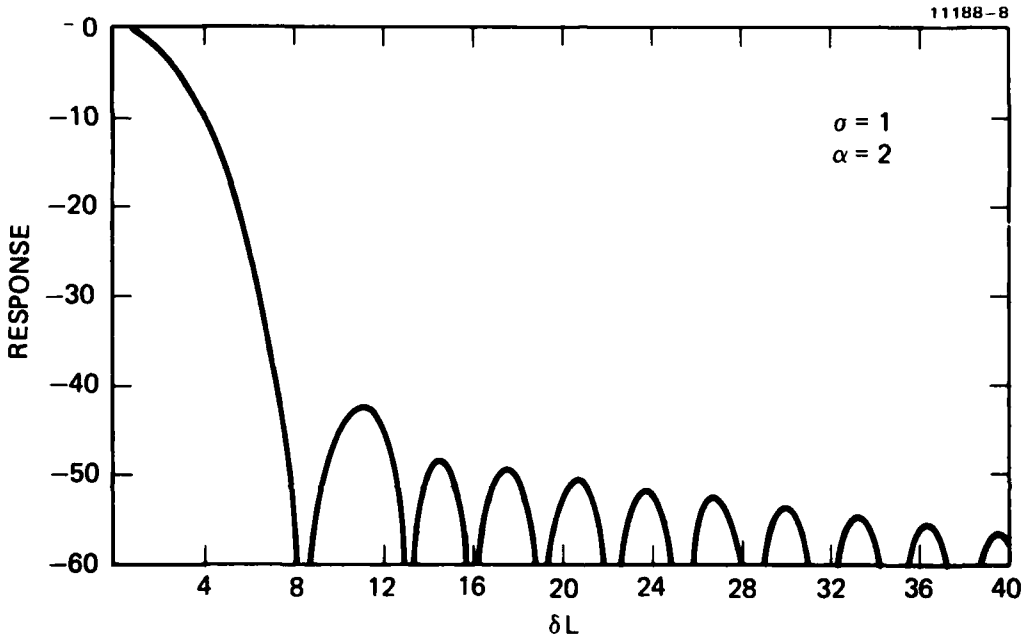

Figure 11(a). Filter response of a Gaussian taper approximated by tangential segments; $\sigma = 1$ and $\alpha = 2$.

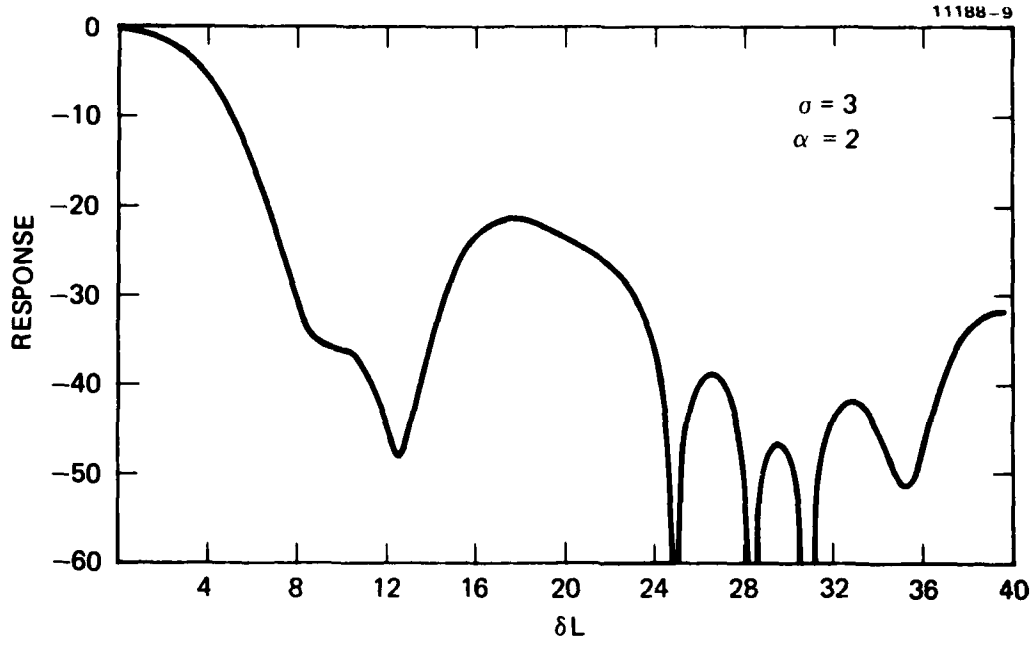

Figure 11(b). Filter response of a Gaussian taper approximated by tangential segments; $\sigma = 3$ and $\alpha = 2$.

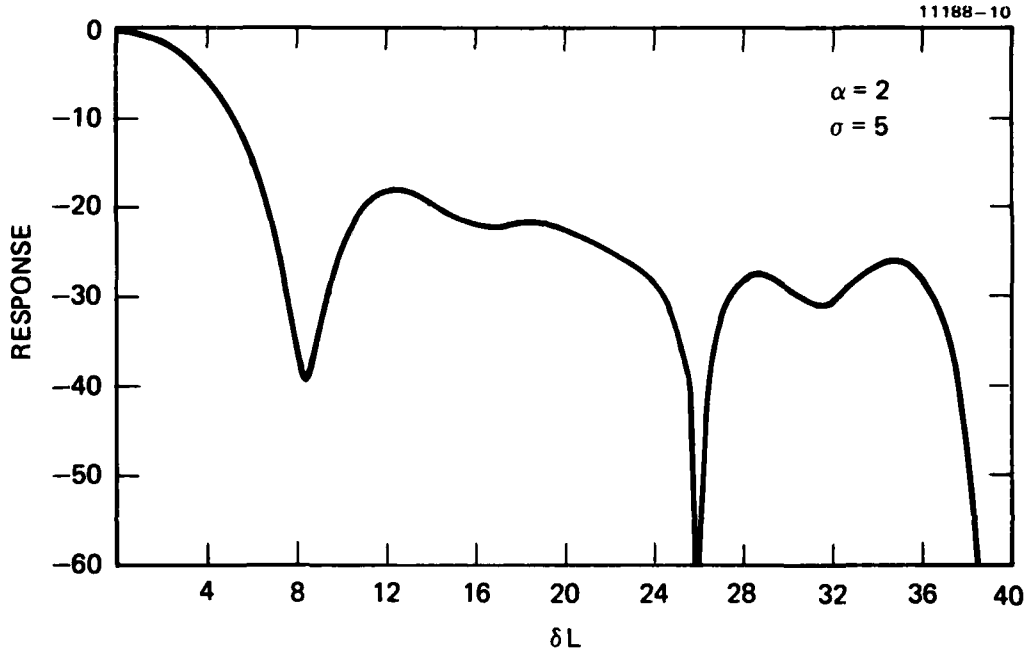

Figure 11(c). Filter response of a Gaussian taper approximated by tangential segments; $\sigma = 5$ and $\alpha = 2$.

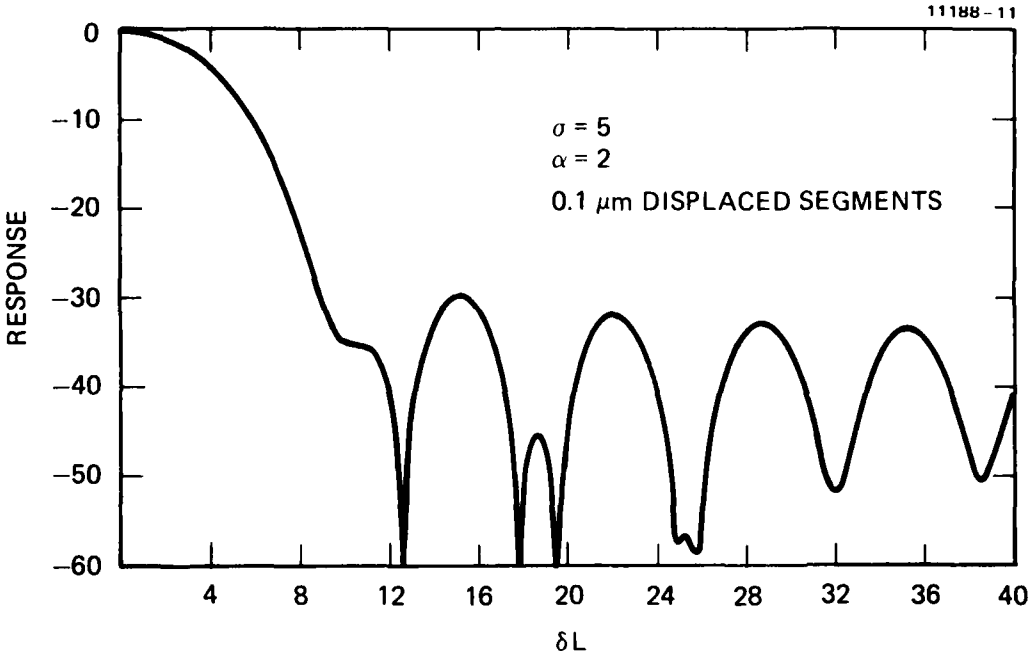

Figure 12. Filter response of a Gaussian taper approximated by 0.1 μm displaced segments; $\sigma = 5$ and $\alpha = 2$.

former fit produces the minimum number of discrete discontinuities in the waveguide with no waveguide offsets. The calculated losses for waveguide offsets and bends shown in Figure 13 suggest that the lowest loss device is one fabricated with tangential segments. Further tradeoff between the two fabrication methods are discussed in Section 2.E.

Due to the lower potential loss of the tangential segments, our mask design utilized this fit to the Gaussian taper function; the angular increment was 0.1°. The calculated best ($\alpha = 2$, $\sigma = 3$) fit is shown schematically in Figure 14. The labeled intersection points are listed in Table 3. Figure 9 shows the calculated filter response for this segmented taper function. In order to have some mask flexibility we ordered a mask that contains 11 different waveguide patterns. In these 11 patters the central section length (see Figure 14) was varied from 0.5 L_{cs} to 1.5 L_{cs}, where L_{cs} is the length of the nominal design central section. The 11 central section lengths are listed in Table 4. The new segment intersection points are presented in Table 3. The filter response for these different patterns have been calculated, and all satisfied the design criteria of the program. The actual waveguide mask layout is shown in Figure 15.

G. MULTIPLE SECTION $\Delta\beta$ REVERSAL ELECTRODE DESIGN

Another advantage of the multiple section $\Delta\beta$ reversal polarization independent switch over the two-section switch around $\sigma = 1$ is an extension of the waveguide fabrication tolerance by versatile electrode design. For example, assuming $\sigma \cong 5$, and $\sigma > 5$ then a six-section electrode can be used. However, if $\sigma < 5$, then a four-section electrode is required to achieve the minimum crosstalk cross-state. (See Figure 16.)

The length of the $\Delta\beta$ reversal segments are not equal, as in the non-tapered switch, due to the variation of κ with z. The length of the segments is determined by the requirement,

$$\int w dt = \frac{L}{N} \quad , \tag{23}$$

where the integral is over the length of the segment, and N is the number of segments desired. For the left outside segment of the four-section switch,

Table 3. Segment Intersection Points

Point Label (See Figure 14)	Nominal Design X(mm)	Modified Designs X(mm)	y(μm)
a	-2.2843	$-L_{cs}/2$ - 1.9098	6.965
b	-1.8723	$-L_{cs}/2$ - 1.4978	4.805
c	-1.1234	$-L_{cs}/2$ - 0.7489	2.195
d	-0.3745	$L_{cs}/2$	0.885
e	2.2843	$-L_{cs}/2$ + 1.9098	0.885
f	-2.2843	$-L_{cs}/2$ + 1.9098	-0.885
g	0.3745	$L_{cs}/2$	-0.885
h	1.1234	$L_{cs}/2$ + 0.7489	-2.195
i	1.8723	$L_{cs}/2$ + 1.4978	-4.805
j	2.2843	$L_{cs}/2$ + 1.9098	-6.965

Table 4. Length of Central Segments

Device	L_{cs} (mm)
1	0.3745
2	0.4494
3	0.5243
4	0.5992
5	0.6441
6	0.749 (nominal design)
7	0.8239
8	0.8988
9	0.9737
10	1.0486
11	1.1135

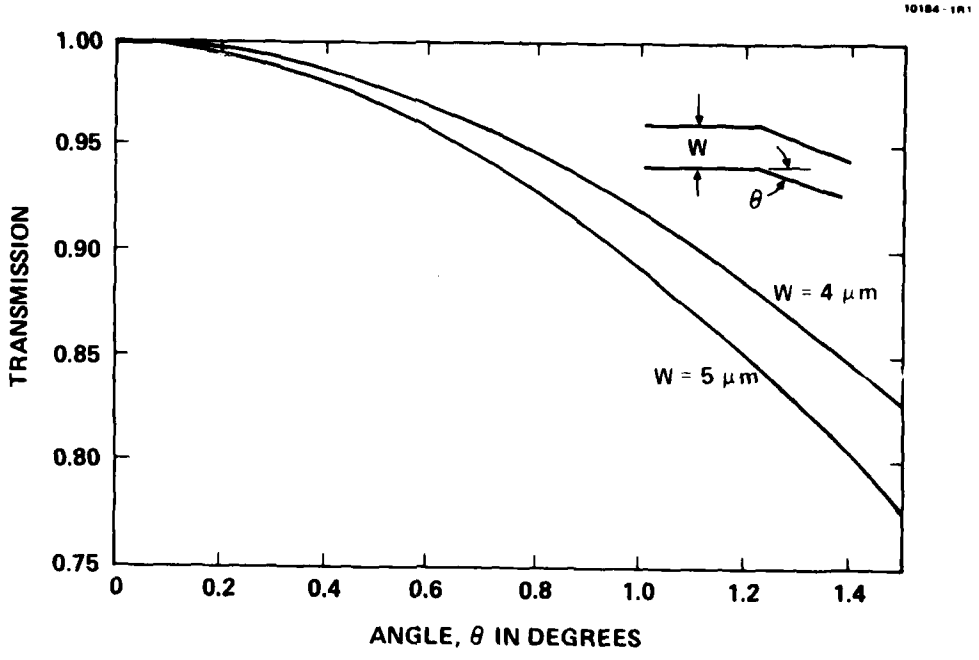

Figure 13(a). Calculated transmission through a waveguide bend formed by the intersection of two straight waveguides.

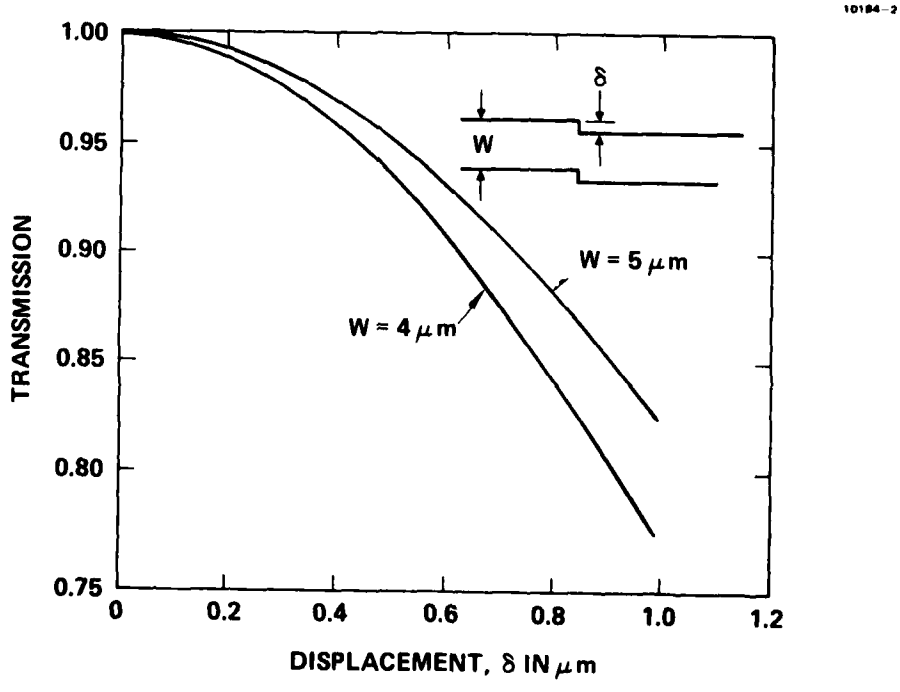

Figure 13(b). Calculated transmission through a waveguide discontinuity formed by a slight lateral displacement.

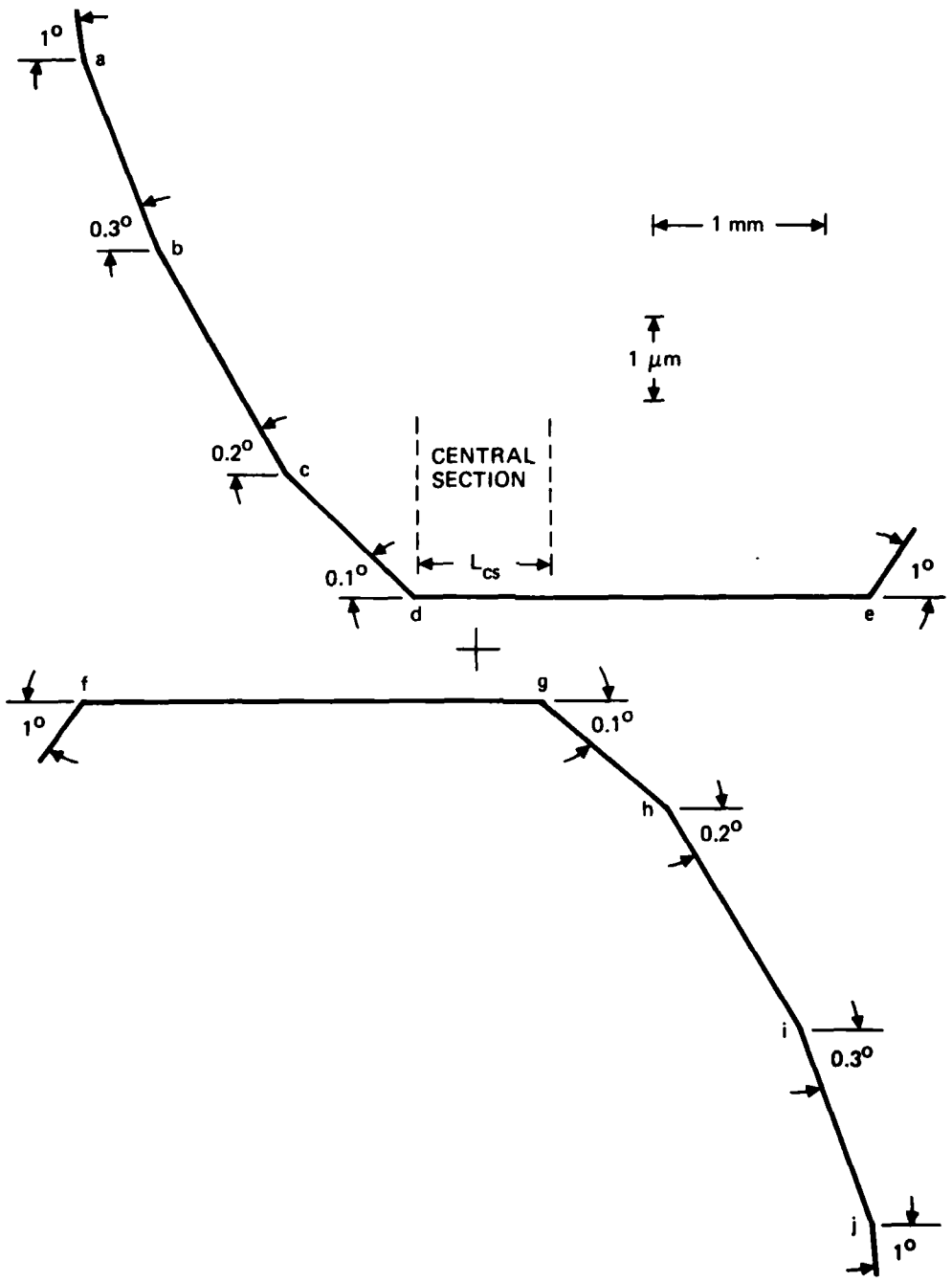

Figure 14. Nominal taper design showing the inner guide boundary. The horizontal scale is 2000 times smaller than the vertical.

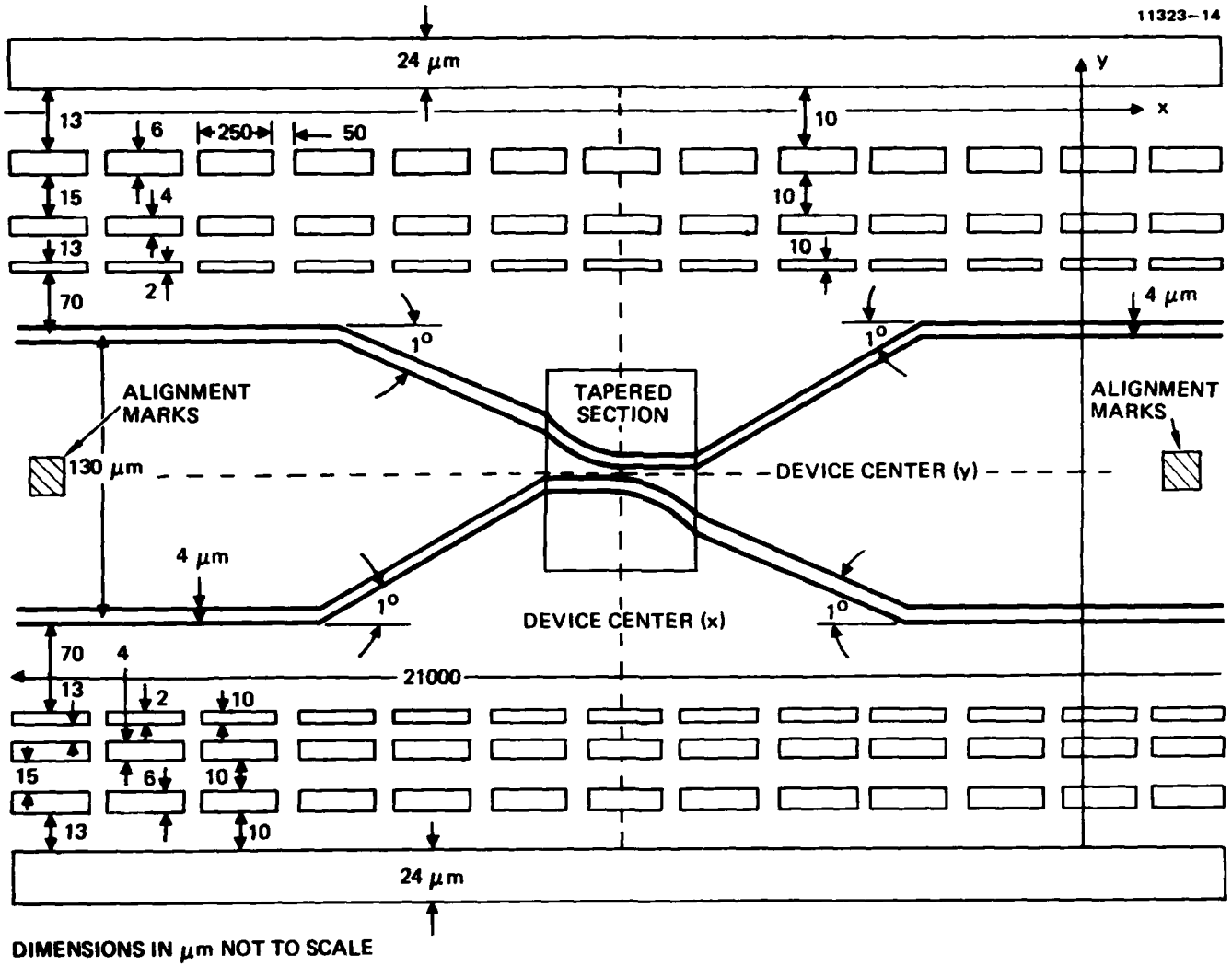

Figure 15(a). Individual device layout.

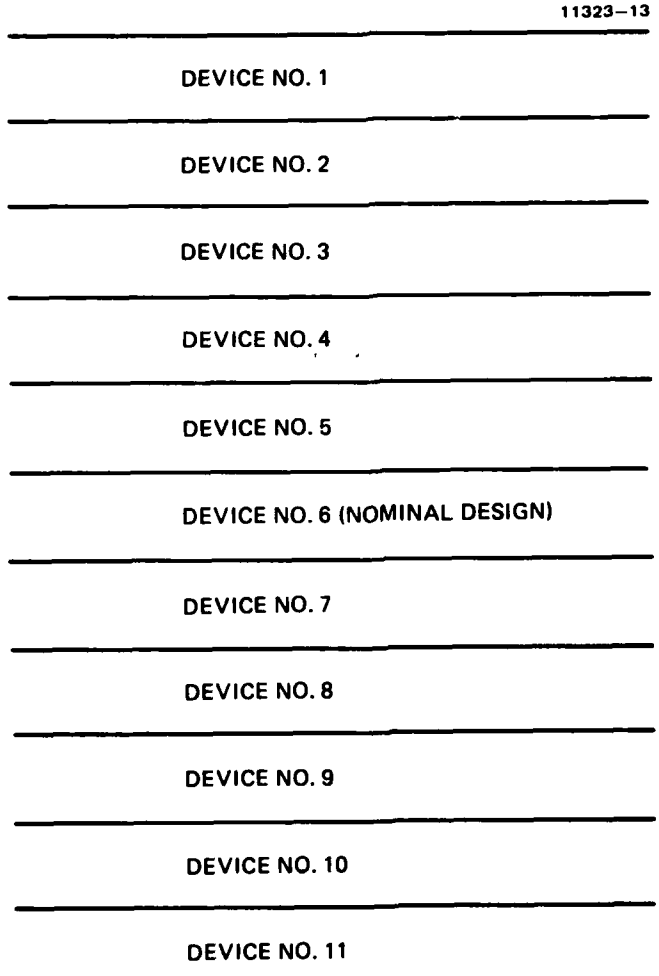

Figure 15(b). Mask layout of eleven devices described in text and Tables 3 and 4.

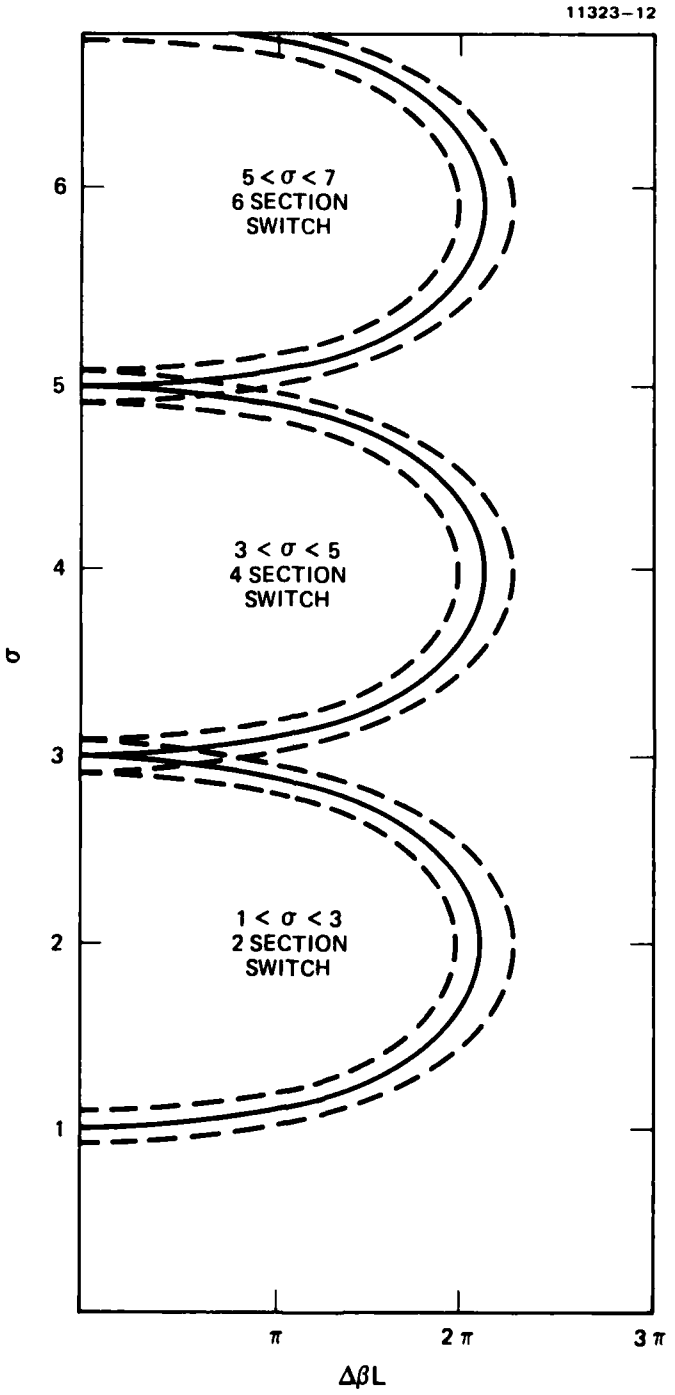

Figure 16. Representation of -20 dB crosstalk limits for different values of σ and number of Δβ reversal switch sections.

$$\int_{-L/2}^{Z} wdt = \frac{L}{2erf(\alpha)} \; erf(\alpha) - \left[erf\left(\frac{2\alpha Z}{L}\right)\right] = L/4 \quad , \tag{24}$$

or

$$\frac{erf(\alpha)}{2} = erf\left(\frac{2\alpha Z}{L}\right) . \tag{25}$$

By approximating erf $(\alpha) \cong 1$ (erf(2) = 0.99532...), we have

$$Z = \frac{0.238L}{\alpha} \quad . \tag{26}$$

A photograph of the four-section electrode fabricated for this program is shown in Figure 17. The electrode was designed assuming $\sigma > 3$; in the event that $\sigma < 3$ in the waveguide device, the electrode has to be modified, as shown in Figure 18. This modification allows two-section reversal switch operation.

The required potentials to be applied to the electrodes to obtain the cross-state $\sigma > 3$, the cross-state $\sigma < 3$, and the parallel state are shown in Figure 19(a) through (c) respectively.

11323-4

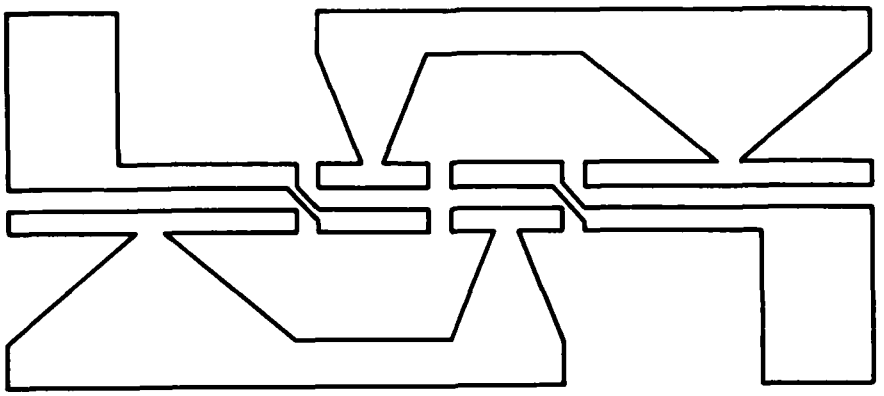

Figure 17. Designed electrode structure which allows four-section $\Delta\beta$ reversal operation.

11323-5

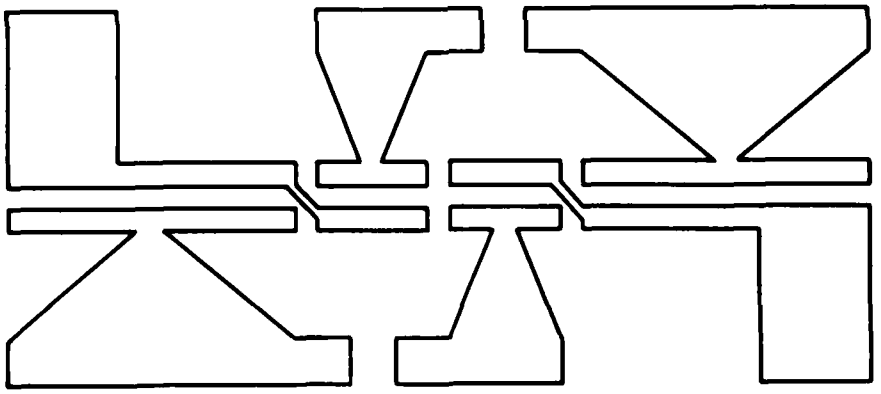

Figure 18. Modified electrode structure which allows two-section $\Delta\beta$ reversal operation.

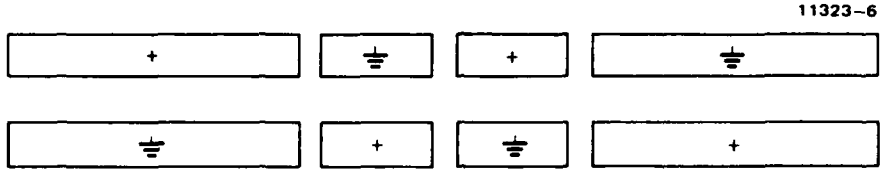

a) 4 SECTION REVERSAL CONFIGURATION ($\sigma > 3$)

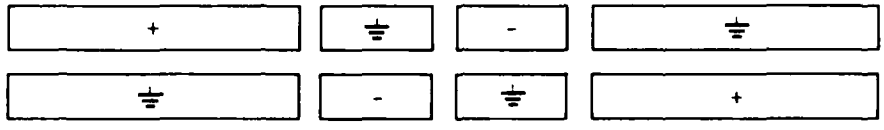

b) 2 SECTION REVERSAL CONFIGURATION ($\sigma < 3$)

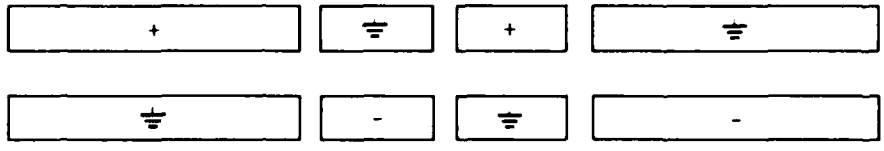

c) UNIFORM ELECTRODE CONFIGURATION

Figure 19. The required potentials to be applied to the electrodes to obtain (a) cross-state of $\sigma > 3$, (b) cross state $\sigma < 3$, and (c) parallel state.

SECTION 3

DELIVERABLE TEST RESULTS

A. INTRODUCTION

Hughes Aircraft has conducted a research and development effort resulting in the demonstration and delivery of three integrated optic polarization independent optic switches operating at 0.83 μm. The switches are electronically switchable with voltage of less than 20 V for the cross state, and approximately 100 V for the parallel state. Less than 20 dB of crosstalk has been demonstrated for both states. The switches have been tested at a frequency of 60 Hz due to a dc drift associated with the presence of a 0.25 μm SiO_2 buffer layer.

The tests conducted on the devices consist of:

- Operational tests;
- Crosstalk isolation of both switching states and polarizations at 0.83 μm;
- Crosstalk isolation at 0.86 μm wavelength for both states.

B. EXPERIMENTAL SET-UP

The experimental set-up for the measurements conducted on the polarization independent switches is shown in Figure 20. The laser diode is mounted and rotated 45° with respect to the $LiNbO_3$ Z axis; this gives equal TE and TM excitation at the input face of the chip, assuming the two modes are of equal size. A polarizer can then be placed before the chip to select either the TE or TM mode for individual polarization operation.

The source of electrical power was a center-tapped variac connected to the 110 V ac output. This provided 60 Hz signals of equal and opposite polarity with respect to ground. Measurements were not conducted at dc due to the drift associated with the presence of the SiO_2 buffer layer.

Relative optical intensities were measured using an APD with a 50 Ω load connected to an oscilloscope.

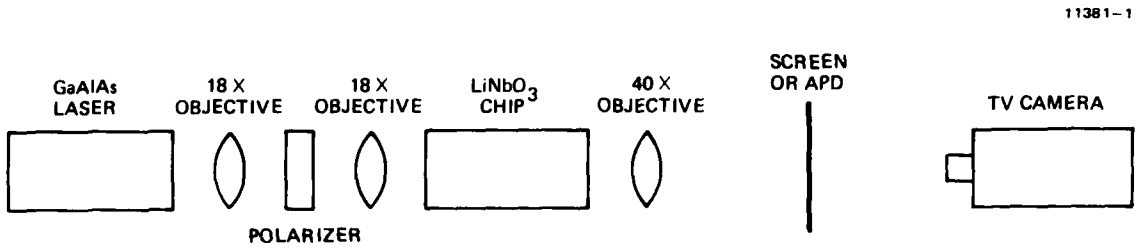

Figure 20. Experimental apparatus.

C. TEST RESULTS

All three delivered items (Nos. 8, 10, 11) have been operationally tested at 0.83 μm. Only one (No. 8) has been tested at the second wavelength and in all possible configurations. The results for item No. 8 are presented and described more thoroughly than for the other devices. The results consist of photographs of the drive signal and detected optical output displayed on an oscilloscope; the electrical connections were in accordance with the electrode discussion in Section 2 and Figure 19.

The first series of photographs (Figure 21) were taken with the electrical configuration shown in Figure 19(c); this corresponds to a constant (i.e., non $\Delta\beta$ reversal) polarity electric field across the whole interaction region. In this configuration the parallel state operation of the switch is demonstrated. The relationship of the optical input and output ports associated with the photographs is illustrated in the figures. The polarization of the input signals is 45°, with respect to the crystal Z axis. The drive signal is displayed at 100 V/div; zero voltage is clearly marked by the cross-over distortion. These photographs clearly point out the following characteristics of the device:

- The device is near a cross state with zero applied voltage (crosstalk $\sim$-12 dB).
- The device is not perfectly symmetrical with respect to zero applied signal. The amount of asymmetry is device dependent, and is believed to be due to processing defects.
- The device requires a drive signal larger than 100 V to achieve excellent parallel state crosstalk. Similar devices have had as much as 150 V applied without electrode breakdown. At this increased voltage better than 20 dB crosstalk levels were observed.

Operational data similar to the above is provided on devices Nos. 10 and 11 in Figures 22 and 23, respectively. In Figure 23 the drive signal is shown at 50 V per division, instead of the 100 V/div in other figures.

The filter function behavior of both polarizations for device No. 8 is illustrated in Figure 24. This data was obtained by placing a polarizer between the laser and the chip. This data shows that the majority of the crosstalk at

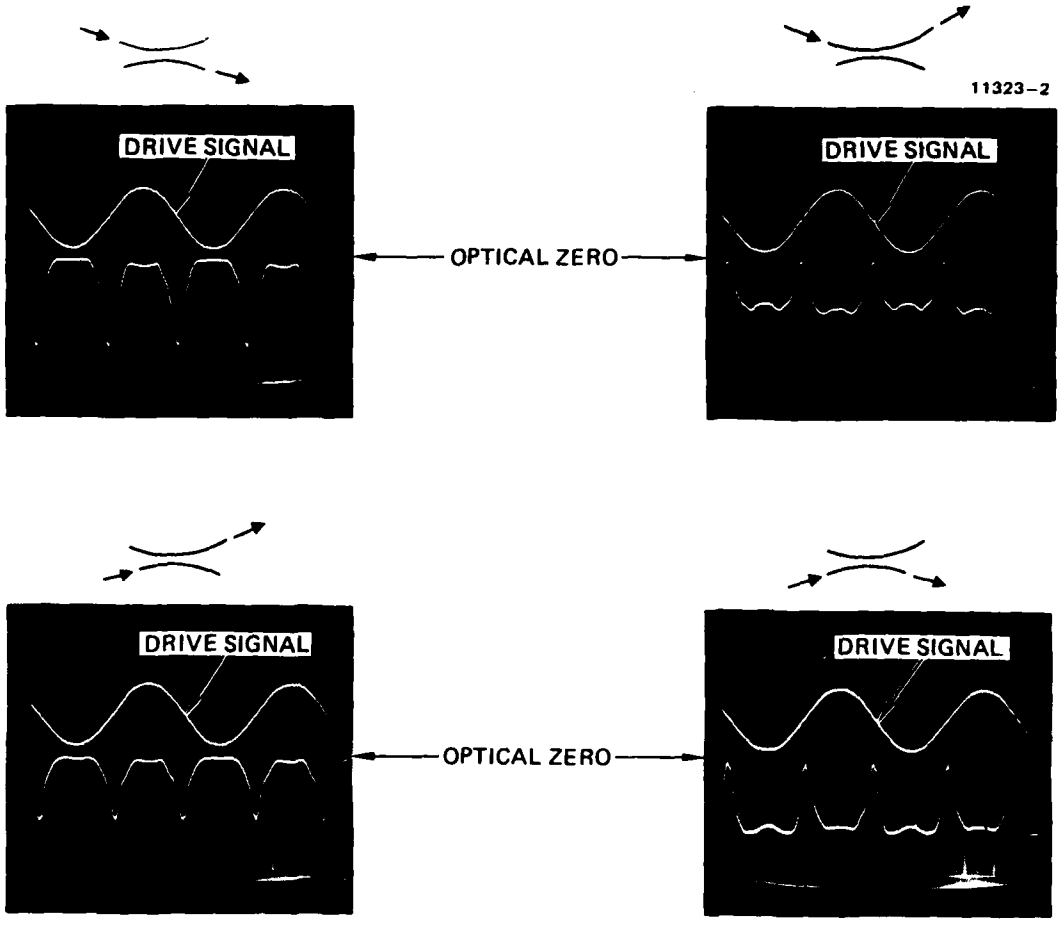

Figure 21. Constant polarity electric field test result for device No. 8 with both TE and TM polarizations excited.

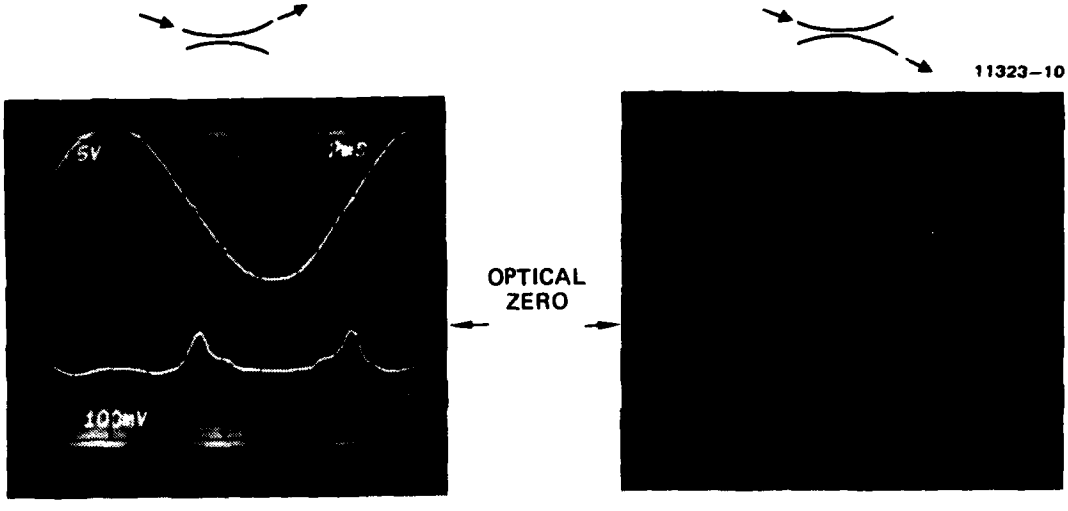

Figure 22. Constant polarity electric field test results for device No. 10 with both TE and TM polarizations excited.

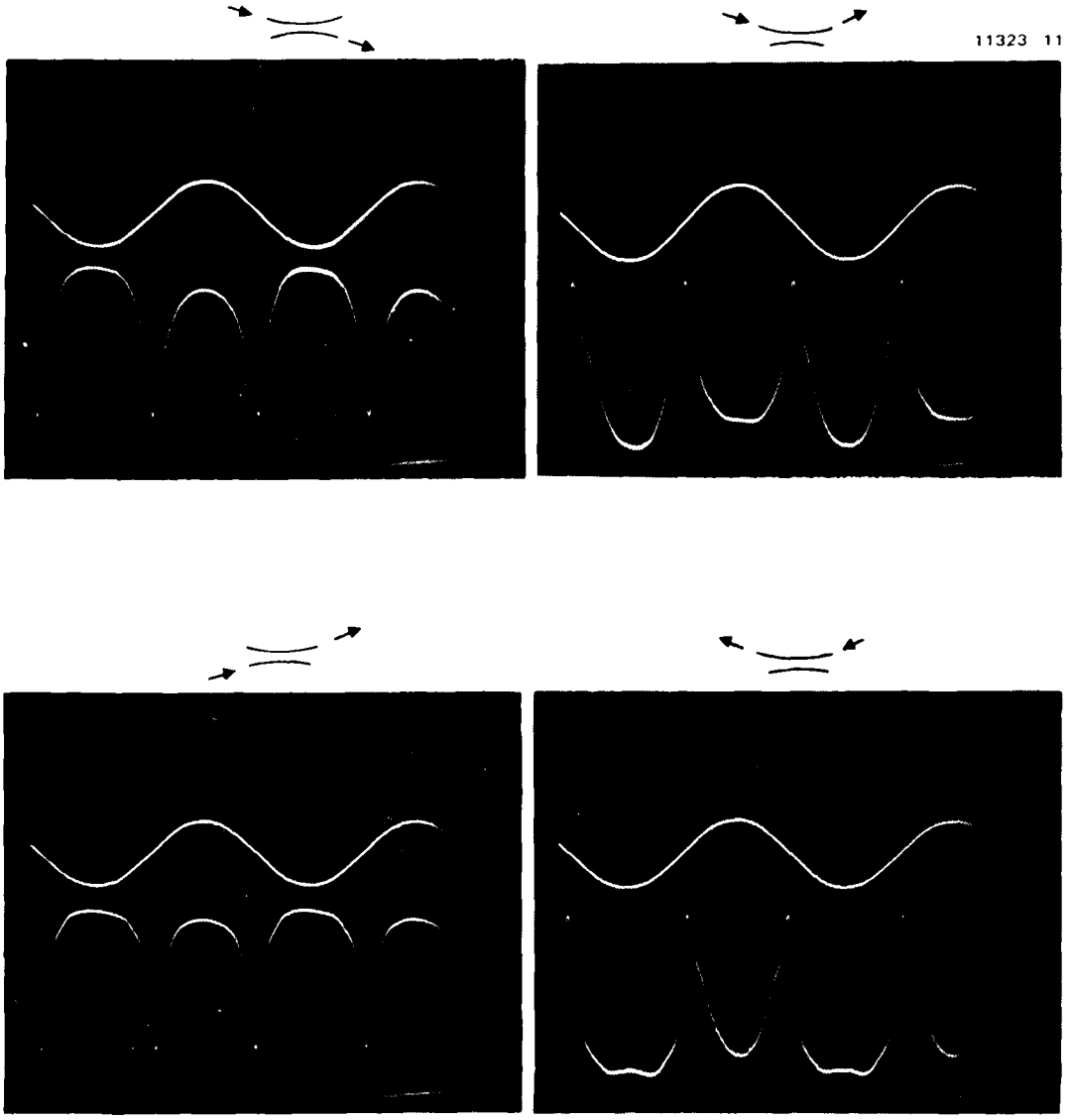

Figure 23. Constant polarity electric field test results for device No. 11 with both TE and TM polarizations excited.

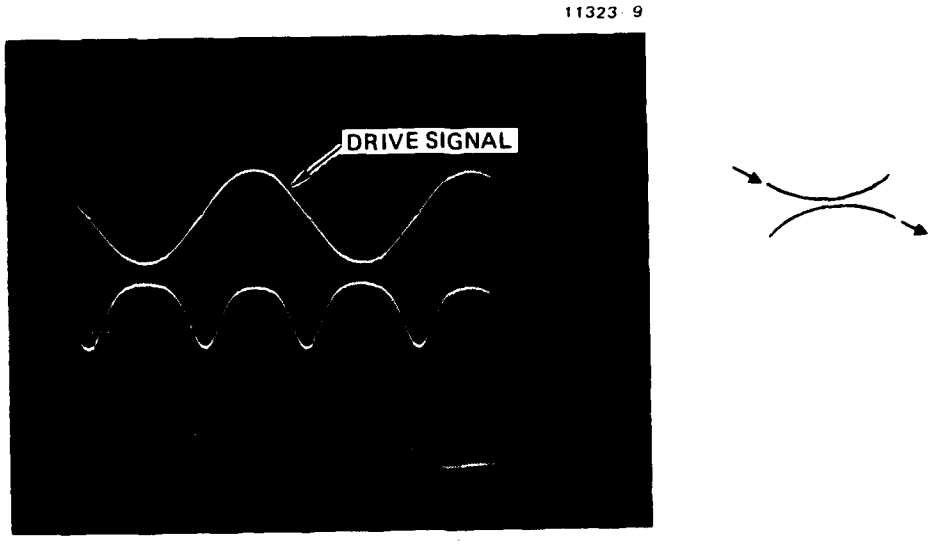

a) TE POLARIZATION ONLY

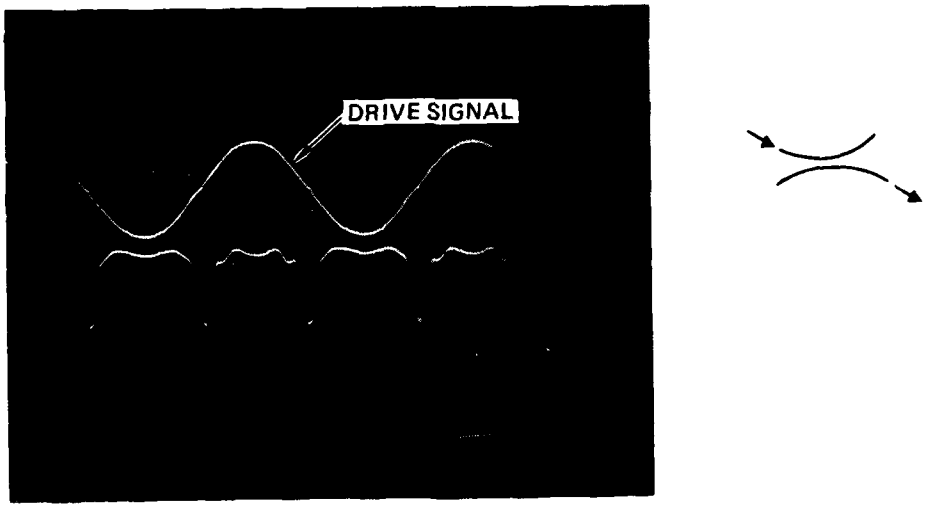

b) TM POLARIZATION ONLY

Figure 24. Individual polarization operation with constant polarity electric field on device No. 8.

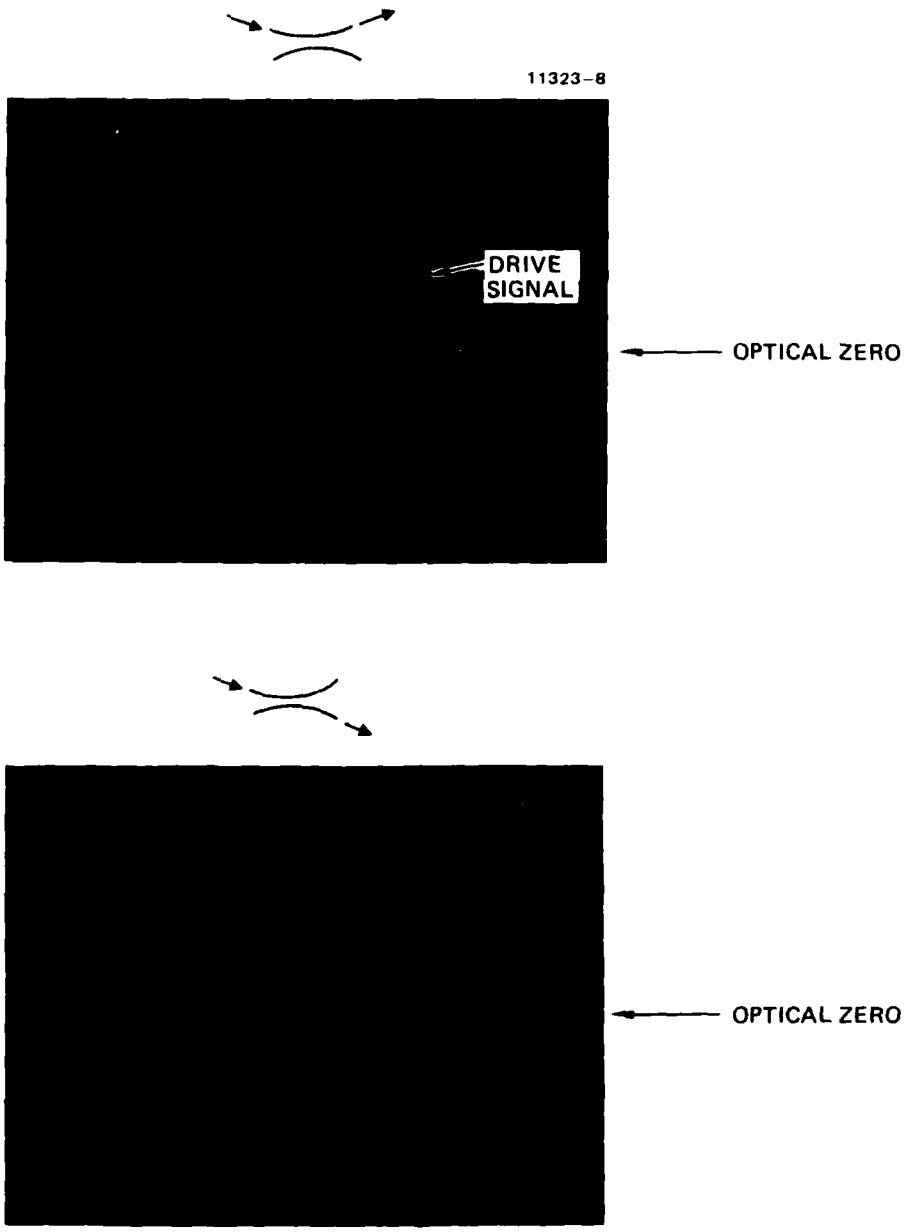

Figure 25. Two-section $\Delta\beta$ reversal test results for device No. 8 showing the cross-state. Both polarizations were excited in the device.

at 100 V is due to the TE polarization, and that increased applied voltage is required to reach the first null in the response.

The next series of photographs were taken with the electrical configuration shown in Figure 19(b); this corresponds to a two section $\Delta\beta$ reversal electrode. In this configuration the cross-state operation of the switch is demonstrated at 0.83 μm wavelength. Using the crossover distortion as a zero voltage reference, improved cross state performance is demonstrated with only a few volts; the drive signal is displayed at 10 V/div. The asymmetry of the device is, however, very apparent. With one polarity the minimum crosstalk occurs with ~20 V. The crosstalk level achieved in Figure 25 is ~16 dB.

The series of photographs shown in Figure 26 were taken using a laser source with a wavelength of 0.86 μm. Figures 26(a) and (b) correspond to the uniform electric field excitation (Figure 19(c)) and demonstrate the parallel state operation at this longer wavelength. Figures 26(c) and (d) correspond to the four-section $\Delta\beta$ reversal electrode configuration (Figure 19(a)) and demonstrate an enhanced cross-state with an applied field. This represents a change in character of the cross-state from the 0.83 μm results, which required a two-section $\Delta\beta$ electrode to enhance the cross state. The character change is easily explained. At the longer wavelength the guide is closer to cut-off; this increases κ, and hence, increases s (Equation 20)) from slightly less than $3\pi/2$ to slightly more than $3\pi/2$. By referring to Figure 16 we see that this will result in the above character change.

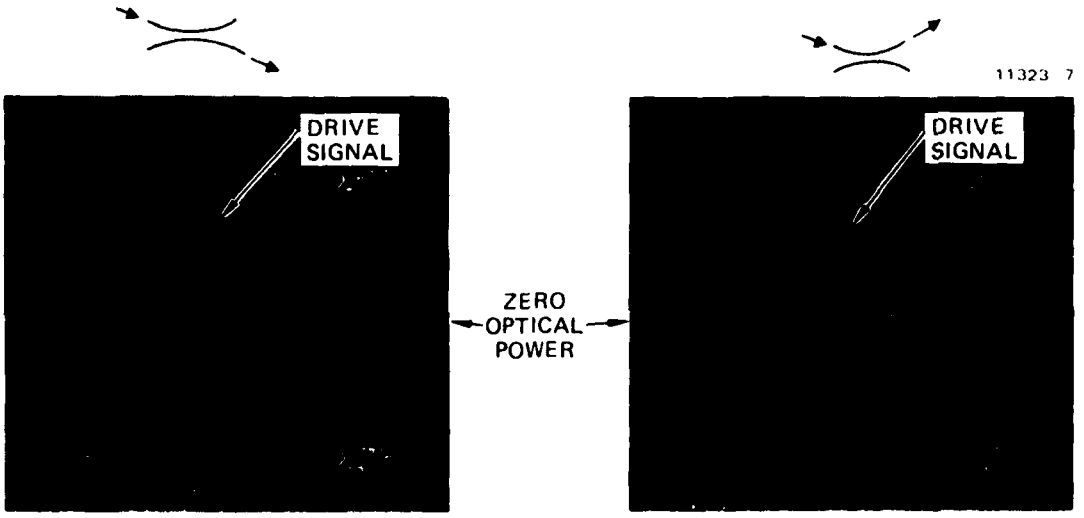

a) PARALLEL ELECTRODE CONFIGURATION

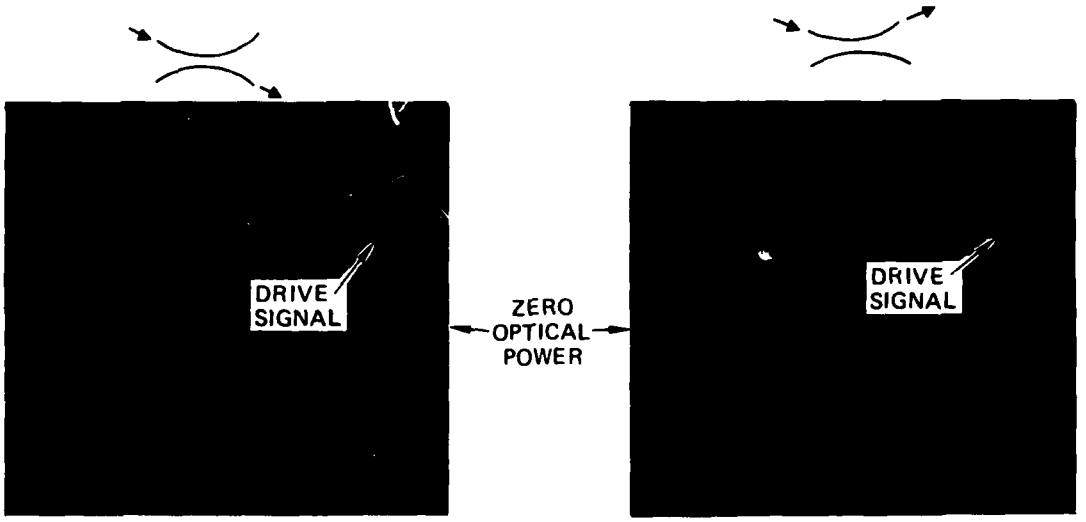

b) CROSS ELECTRODE CONFIGURATION

Figure 26. Test results for device No. 8 at 0.86 μm wavelength.

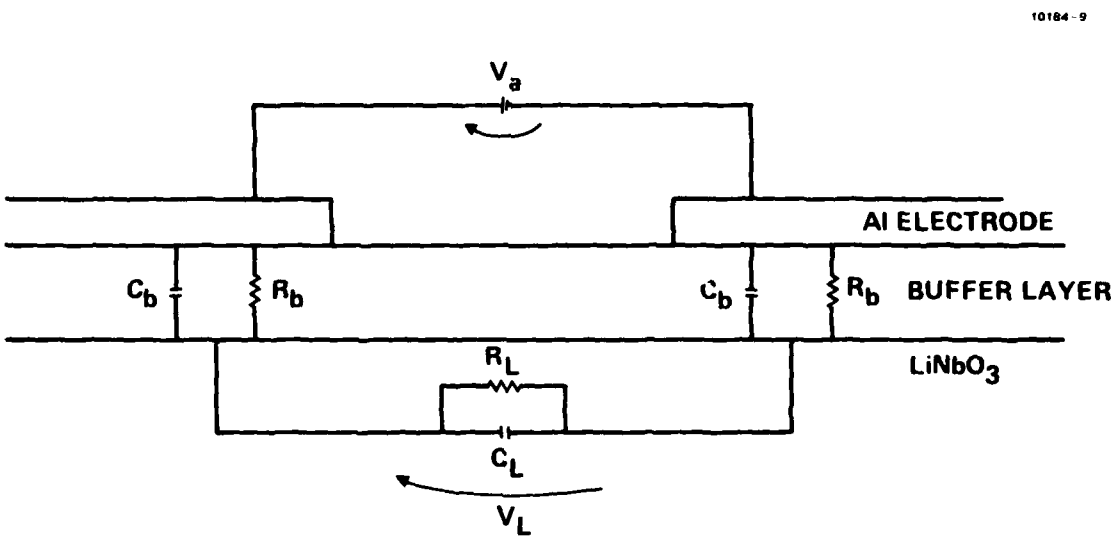

IF $R_b \gg R_L$ $V_L \approx$ 0 UNDER DC OPERATION (SiO_2 OPERATION)

IF $R_L \gg R_b$ $V_L \approx V_a$ UNDER DC OPERATION (TiO_2 OPERATION)

Figure 27. Equivalent circuit model of $LiNbO_3$-buffer layer electrode configuration.

SECTION 4

RECOMMENDATIONS AND CONCLUSIONS

A. INTRODUCTION

This highly successful program has resulted in the demonstration of a polarization independent switchable directional coupler. Although the device operates according to the theoretical design, there are some areas where additional research is required. The program included several noteworthy accomplishments:

- A four-section $\Delta\beta$ reversal polarization independent switch in the 0.83 to 0.86 μm wavelength range was designed, fabricated and demonstrated.
- The filter characteristics of a Gaussian taper function was investigated theoretically and experimentally.
- Experimental elimination of the Li_2O out-diffused mode using a H_2O bubbler with device incorporation was demonstrated.

Based on this extensive work we recommend that additional research be conducted in the following areas:

- Device design and fabrication techniques in order to reduce switch voltage, waveguide losses, and polarization noise.
- Buffer layer development to allow dc switch operation.
- Device pigtailing.

These areas are discussed below.

B. DEVICE DESIGN

The many aspects of device design have been discussed in Section 2E. In general, the switching voltage can be reduced most effectively by increasing the integrated coupling length. At the beginning of this contract the minimum displacement discontinuity achievable (by Electromask) for a waveguide switch of this nature was approximately 0.5 μm. Since then, Electromask has purchased a new digitizing system which will allow 0.1 μm displacement discontinuities for

parallel segments. As pointed out in Section 2E, this will theoretically allow designs with larger s values, which increases coupling length, and thus reduces switching voltages.

Another area that should be more thoroughly investigated is the optical noise generated by the differential attenuation of the two polarizations in the chip. The two nearly degenerate modes (polarizations) in single mode fiber are coupled together by small fiber defects, microbends, and environmental perturbations that are constantly changing, due to environmental changes. This continuously changing polarization, when coupled to the IO chip, will produce noise due to the differential attenuation of the TE and TM modes. This noise exists in both the switching states, but the magnitude may be state dependent.

C. BUFFER LAYER

The presence of a buffer layer has important ramifications on low-frequency operation. This follows because the buffer layers and the $LiNbO_3$ typically have different resistivities. This can be demonstrated with a simple equivalent circuit model, as shown in Figure 27. The model includes three capacitors with corresponding leakage resistors. Two capacitors are across the buffer layer and one is across the $LiNbO_3$. This is equivalent to having three dielectrics with different leakage resistances between the plates of a parallel plate capacitor. At dc operation, the voltage across the three capacitors or dielectrics is a simple voltage division of the leakage resistances. If the resistance across the $LiNbO_3$, R_L, is much less than the resistance of the two buffer layer regions, R_b, then in dc operation there will be only a small voltage or corresponding electric field across the $LiNbO_3$. Note that R_L is a distributed resistance which takes into account the $LiNbO_3$, the $LiNbO_3$ Si interface, and in part, the Si buffer layer. Conversely, if the resistance associated with the buffer layer, R_b, is small compared to R_L, the electric field and associated voltage will be largest in the $LiNbO_3$.

Other research labs have had good results in this area by either annealing the samples in an O_2 atmosphere after the buffer layer deposition, or by removing the buffer layer in the electrode gaps. Both of these solutions suggest that the resistance associated with the SiO_2 is too low. Additional work in this area is required to define the problem.

D. DEVICE PIGTAILING OPTIMIZATION

In this research the device was designed based upon coupler characteristics independent of fiber pigtailing considerations. Research should be aimed at fabricating a device with waveguides optimized for fiber pigtailing instead of selecting the guides which give the highest probability of device success. This program has shown that the fabrication tolerances are such that the nominal design can be reasonably achieved, and suggests that devices can be easily made with less optimum guides from a device consideration.

Another area of necessary research is the development of edge AR coating techniques. Although HRL has successfully designed, deposited, and tested AR coating on $LiNbO_3$, the quality of the coatings near the edge have not been adequate for low reflectance fiber pigtails.

REFERENCES

1. .C. Alferness, Appl. Phys. Lett. 35, 748 (1979).

2. R.V. Schmidt and H. Kogelnik, Appl. Phys. Lett. 28, (1976).

3. J.M. Hammer, in Integrated Optics, edited by T. Tamer (Springer, Heidelberg, 1975).

4. R.C. Alferness, R.V. Schmidt, and E.H. Turner, Appl. Opt. 18, 4012 (1979).

5. H. Kogelnik and R.V. Schmidt, IEEE J. Quantum Electron., QE-12, 396 (1976).

6. R.C. Alferness, Appl. Phys. Lett. 35, 260 (1979).

7. J.L. Juckel, V. Ramaswamy, S.P. Lyman, A.M. Glass, and D.H. Olson – paper WB3 "Elimination of Out-Diffused Surface Guiding in Ti-Diffused $LiNbO_3$" IOOC 81 Technical Digest (Apr. 27-29, 1981), San Francisco, California.

8. E. Marcatili, Bell System Tech. J. 48, 2071-2102 (1969).

9. H. Kogelnik, "Filter Response of Non-Uniform Almost-Periodic Structure," Bell Systems Technical Journal, Vol. 55, 109 (1976).

10. P.S. Cross and H. Kogelnik, "Sidelobe suppression in corrugated-waveguide filters," Optics Lett. 1, 43 (1977).

11. R.C. Alferness and P.S. Cross, "Filter Characteristics of Codirectionally Coupled Waveguides with Weighted Coupling," IEEE J. Quantum Electron. QE-14, 843 (1978).

12. R.C. Alferness, "Optical directional couplers with weighted coupling," Appl. Phys. Lett. 35, 260 (1979).

13. M. Matsuhara, K.O. Hill,and A. Watanabe "Optical-waveguide filters: Synthesis," JOSA 65, 804, 1975.

14. R.C. Alferness and R.V. Schmidt, "Tunable optical waveguide directional coupler filter," presented at the topical meeting Integrated and Guided Wave Optics, June, 1978; also in Appl. Phys. lett. 33, 161-163 (1978).

15. R.C. Alferness, R.V. Schmidt and E.H. Turner, "Characteristics of Ti-diffused lithium niobate optical directional couplers," Appl. Optics 18, 4012 (1979).


FILMED
8